

Spatial Interference Cancellation for Multi-Antenna Mobile Ad Hoc Networks

Kaibin Huang, Jeffrey G. Andrews, Robert W. Heath, Jr.,
Dongning Guo, and Randall A. Berry

Abstract

Interference between nodes is a critical impairment in mobile ad hoc networks (MANETs). This paper studies the role of multiple antennas in mitigating this interference. Specifically, a network is studied in which transmitters opportunistically transmit and zero-forcing beamforming is applied at each receiver for canceling the strongest interferers. The performance of this approach is analyzed by evaluating the *transmission capacity* of a network with Poisson distributed transmitters and i.i.d. Rayleigh fading channels. This metric corresponds to the maximum density of transmitting nodes subject to an outage constraint for a given signal-to-interference ratio (SIR). Mathematical tools from stochastic geometry are applied to obtain scaling laws for the transmission capacity and characterize the impact of inaccurate channel state information (CSI). In particular, for small target outage probabilities, the transmission capacity is proven to increase following a power law, where the exponent is the inverse of the size of each node's antenna array or larger, depending on the path-loss exponent. Moreover, CSI inaccuracy is shown to only decrease the constant in the scaling law of the transmission capacity as the outage probability goes to zero, provided that an appropriate length for the CSI training sequence is used. The needed length of such training is also derived. Numerical results suggest that using merely one additional antenna at each node increases the transmission capacity by an order of magnitude or more, even when the CSI is imperfect.

I. INTRODUCTION

In a mobile ad hoc network (MANET), the mutual interference between nodes poses a fundamental limit on the throughput of peer-to-peer communication. One approach for mitigating the effect of interference is to provision the nodes in a MANET with multiple antennas and use the spatial degrees of freedom

K. Huang is with Department of Electronic and Computer Engineering, Hong Kong University of Science and Technology, Hong Kong; J. G. Andrews, and R. W. Heath Jr. are with Wireless Networking and Communications Group, Department of Electrical and Computer Engineering, The University of Texas at Austin, 1 University Station C0803, Austin, TX 78712-0240; D. Guo and R. A. Berry are with Department of Electrical Engineering & Computer Science, Northwestern University, Evanston, IL 60208. Email: khuang@mail.utexas.edu, {rheath, jandrews}@ece.utexas.edu, dguo@northwestern.edu. K. Huang was the recipient of the University Continuing Fellowship from The University of Texas at Austin. This work is funded by the DARPA IT-MANET program under the grant W911NF-07-1-0028, the National Science Foundation under grants CCF-514194, CNS-435307, and CCF-0644344, and ARO grant W911NF-06-1-0339.

created by these antennas to cancel a portion of the interference. We consider such an approach in this paper. Namely, each receiver uses zero-forcing beamforming to attempt to cancel the interference from the strongest interferers. Each transmitter simply chooses a random beam and transmits according to a threshold rule as in [1]. This approach requires only limited local coordination making it suitable for a MANET. A basic question is then to quantify the gains in network performance as a function of the system parameters. Furthermore, implementing this approach requires some amount of channel state information (CSI) at each receiver. In a MANET environment, there will naturally be inaccuracy in this CSI. A second key question is then to determine how this inaccuracy will impact the network performance.

We provide answers to both of the above questions in terms of the *transmission capacity* of a simple network consisting of Poisson distributed transmitters and spatially i.i.d. Rayleigh fading. This metric, introduced in [2], is defined as the maximum density of transmitters so that a typical transmitter will satisfy an outage probability constraint for a target signal-to-interference-and-noise ratio (SINR).¹ By studying the scaling of transmission capacity as the outage probability goes to zero, we are able to quantify the gains in network performance due to spatial interference cancellation as a function of the relevant system parameters, as well as the effect of CSI inaccuracy. These results suggest that multiple antennas can significantly improve the performance of MANETs, even with inaccurate CSI.

A. Prior Work and Motivation

As noted previously, our primary performance metric is the transmission capacity. For Poisson distributed transmitters, this metric is studied in [2] for single-antenna ad hoc networks assuming fixed transmission power and an ALOHA-like medium access control (MAC) layer. Transmission capacity has also been used to make a tractable analysis of opportunistic transmissions [1], distributed scheduling [3], coverage [4], network irregularity [5], bandwidth partitioning [6], and successive interference cancellation (SIC) [7] in ad hoc networks. Additionally, in [1], transmission capacity is analyzed for several models of multi-antenna ad hoc networks. The work in [1] differs from this paper in that the antennas are not used for interference cancellation, but rather for interference averaging through different multiple antenna diversity techniques.

As discussed in [1], [2], transmission capacity is closely related to the notion of *transport capacity* introduced in [8] and further studied in a number of papers including [9]–[13]. Transport capacity focuses on the scaling of a network’s total end-to-end throughput per unit distance as a function of the network’s size, while our focus here is on the number of single-hop transmissions as a function of the transmitter density. Furthermore, most work on transport capacity assumes perfect scheduling and zero-outage, while here we focus on a random access model with outages.

¹This metric focuses on the one-hop performance of a MANET and does not explicitly account for multi-hop routing.

In addition to spatial interference cancellation, there are a number of other possible approaches for mitigating interference in MANETs. For example, the *interference alignment* approach in [14] achieves the optimal number of degrees of freedom in a high signal-to-noise ratio (SNR) setting. This approach appears daunting in practice because it requires jointly designed precoders and perfect CSI of interference channels. In contrast, the approach considered here only requires “local” channel state information and no coordination of transmit precoders. Another method for interference management, used in many practical MAC protocols, is to create an interferer-free area – a *guard zone* – around each receiving node through carrier sensing. As shown in [3], by optimizing the guard-zone size, this method leads to significant gain in a single-antenna MANET’s transmission capacity with respect to purely random access. Here, the use of interference cancellation, can be viewed as creating an effective guard zone for each receiving node, without requiring that other nearby transmitters are suppressed.

A number of other recent papers have addressed other aspects of multi-antenna MANETs. For example, beamforming or directional antennas [15] have been integrated with the MAC protocols for MANETs to achieve higher network spatial reuse or energy efficiency [16]–[28]. In addition, multi-antenna techniques have been shown to improve the efficiency of routing protocols for MANETs [29]–[33]. Directional antennas have been studied for suppressing interference in MANETs by spatial filtering [23]–[27]. Directional antennas are only suitable for environments with sparse scattering. In contrast, beamforming is suitable for both sparse and rich scattering, and is hence adopted in this paper as well as in [18]–[20], [28] for spatial interference cancellation. Most prior work focuses on designing MAC protocols and relies on simulations for investigating network throughput [16]–[27]. The capacity of MANETs with beamforming or directional antennas are analyzed in [34]–[36]. In [34], [35], the use of directional antennas are shown to increase the linear scaling factor of network transport capacity. In [36], the transmission capacity for multi-antenna MANETs is analyzed, where interference is treated as noise and suppressed by averaging through beamforming. In view of prior work, there still lacks of theoretic characterization of the relationship between the transmission capacity of MANETs and spatial interference cancellation. Furthermore, the important issue of how CSI inaccuracy affects the throughput of MANETs has not been analyzed in [16]–[27], [34]–[36].

B. Contributions and Organization

Our main contributions are summarized as follows. This paper targets a MANET with single-stream data links and perfect symbol synchronization between nodes. First, we give an approach for using zero-forcing beamforming to cancel interference in a MANET and thereby improve network transmission capacity².

²The zero-forcing method is used for analytical simplicity, and the extension to minimum-mean-squared-error (MMSE) beamforming is straightforward.

The number of canceled interferers depends on the number of antennas at each receiver. Moreover, transmit beamforming vectors are randomly selected to avoid iterative receive beamforming and potential network instability. Second, assuming Poisson distributed transmitters and spatially i.i.d. Rayleigh fading channels, bounds on the signal-to-interference ratio (SIR) outage probability are derived for the case of perfect and imperfect CSI. These bounds are found to be reasonably tight and lead to bounds on the network transmission capacity. Third, the scaling laws for transmission capacity are derived for asymptotically small target outage probability. Specifically, with interference cancellation, the asymptotic transmission capacity grows according to a power law for both perfect and imperfect CSI. The base of the power law is the target outage probability, and the exponent is the inverse of the antenna-array size if it is smaller than the path-loss exponent. Otherwise, the exponent is bounded between the inverse of the antenna-array size and that of the path-loss exponent. Finally, the required lengths of CSI training sequences are derived for constraining the outage probability to be within a multiplicative factor of that with perfect CSI and for achieving a nearly optimal scaling law of the transmission capacity, respectively. These results are useful for evaluating the amount of CSI overhead needed to control the degree of network performance degradation due to CSI inaccuracy.

Simulation results are also presented. As observed from these results, employment of a few (two to four) antennas per node is sufficient for harvesting most of the capacity gains promised by spatial interference cancellation. In particular, compared with the case of single antennas, a capacity gain of more than an order of magnitude can be achieved by using only one additional antenna at each node, even if CSI is imperfect. Moreover, a moderate length CSI training sequence is observed to be sufficient for keeping the loss of transmission capacity due to CSI inaccuracy small. These results demonstrate the effectiveness of spatial interference cancellation for practical applications.

The remainder of this paper is organized as follows. Section II describes the network and wireless channel models. Section III introduces the algorithm for spatial interference cancellation, and presents the effective network and channel models based on the algorithm. The SIR outage probability and transmission capacity are analyzed for perfect and imperfect CSI in Sections IV and V, respectively. Numerical results are presented in Section VI, followed by concluding remarks in Section VII.

II. NETWORK AND CHANNEL MODELS

A. Network Model

In this paper, the locations of potential transmitting nodes in a MANET, including both active and inactive transmitters, are modeled as a Poisson point process following the common approach in the literature [1], [2], [7], [36], [37]. Specifically, the positions of the potential transmitters form a homogeneous Poisson point process on a 2-dimensional plane with the density denoted by λ_o . Time is slotted and in each time-slot potential transmitting nodes follow a simple ALOHA-like random access protocol, in

which they transmit independently with a fixed probability P_t . Let T_n denote the coordinate of the n th transmitting node. Given the random access protocol, the set $\Phi = \{T_n\}$ is also a homogeneous Poisson point process but with the smaller density $\lambda = P_t \lambda_o$ [38]. Each transmitting node is associated with a receiving node located at a fixed distance denoted as d .³

Consider a typical receiving node located at the origin, denoted as R_0 , and hence $|T_0| = d$. This location constraint of T_0 does not compromise the generality since the transmitting node process Φ is translation invariant. Furthermore, according to Slivnyak's theorem [39], the remaining transmitting nodes, namely $\Phi/\{T_0\}$, remain as a homogeneous Poisson point process with the same node density λ .

The MANET is assumed to be interference limited and thus noise is neglected for simplicity.⁴ Consequently, the reliability of data packets received by the node R_0 is determined by the SIR. Moreover, we assume that each data link in the network has a single stream, and communications between nodes are perfectly synchronized in symbols. All transmitting nodes are assumed to use uniform transmission power, P_D . Let S denote the random power factor for the link from T_0 to R_0 so that the received power at R_0 is SP_D . Likewise, let S_n represent the interference power factor from transmitting node T_n to R_0 , so that the received interference power at R_0 due to T_n is $I_n = S_n P_D$. Thus, the SIR at R_0 is given as

$$\text{SIR} = \frac{S}{\sum_{T_n \in \Phi/\{T_0\}} I_n}. \quad (1)$$

Since the SIR is independent of P_D , $P_D = 1$ is assumed for simplicity. The correct decoding of received data packets requires the SIR to exceed a threshold θ , which is identical for all receiving nodes. In other words, the rate of information sent from a transmitter to a receiver is no less than $\log_2(1 + \theta)$ assuming Gaussian signaling. To support this information rate with high probability, the outage probability that SIR is below θ must be no greater than a given threshold $0 < \epsilon < 1$, i.e.

$$P_{\text{out}}(\lambda) = \Pr(\text{SIR} \leq \theta) \leq \epsilon \quad (2)$$

where $P_{\text{out}}(\lambda)$ denotes the SIR outage probability as a function of λ . Given an outage constraint ϵ , P_{out} determines the transmission capacity, which is defined as [2]

$$C(\epsilon) = (1 - \epsilon)\lambda_\epsilon \quad (3)$$

where $P_{\text{out}}(\lambda_\epsilon) = \epsilon$. Note that this equality maximizes transmission capacity under the outage constraint (2) since $P_{\text{out}}(\lambda_\epsilon)$ increases monotonically with λ_ϵ .

³More generally, the distances between receivers and their corresponding transmitters could also be randomly distributed. However, as shown in [1], randomness in these distances has no significant effect on the analysis of transmission capacity and is thus omitted for simplicity.

⁴Addressing the effect of noise requires straightforward but maybe tedious modifications of the analytical results in this work. In particular, accounting for noise changes only the linear factors in the asymptotic scaling laws for transmission capacity in Theorem 2.

B. Channel Model

We adopt a narrow-band channel model with frequency-flat block fading, which is common in the literature (see, e.g., [2], [37], [40], [41]). During each transmission attempt the fading realization is assumed to stay fixed. Each node in the network is equipped with L antennas. Consequently, there exists a $L \times L$ multiple-input-multiple-output (MIMO) channel between every pair of nodes. Each MIMO channel consists of path-loss and spatially i.i.d. small fading components, corresponding to rich scattering. Specifically, the channel from a node T_n to the typical receiving node R_0 is $\mathbf{H}_n = r_n^{-\alpha/2} \mathbf{G}_n$. The factor $r_n^{-\alpha/2}$ represents path-loss, where $r_n = |T_n|$ is the Euclidean distance and $\alpha > 2$ is the path-loss exponent. The factor \mathbf{G}_n , is a $L \times L$ matrix of i.i.d. $\mathcal{CN}(0, 1)$ components, modeling spatially i.i.d. Rayleigh fading. Each transmitter is assumed to send a single spatial data stream so that stream control [42] is unnecessary and beamforming is applied at each transmitter and receiver. Let \mathbf{f}_n and \mathbf{v}_0 denote the beamforming vectors at T_n and R_0 , respectively. Then the effective channel power for the data link from T_0 to R_0 is $S = |\mathbf{v}_0^\dagger \mathbf{H}_0 \mathbf{f}_0|^2$, and that for the interference link from T_n to R_0 is $S_n = |\mathbf{v}_0^\dagger \mathbf{H}_n \mathbf{f}_n|^2$.

III. SPATIAL INTERFERENCE CANCELLATION: ALGORITHM AND MODELING

The algorithm of zero-forcing beamforming for spatial interference cancellation is first described. The resultant effective network and channel models are discussed for perfect and imperfect CSI, respectively.

A. Perfect CSI

In this section, each receiver is assumed to have perfect CSI of the channel between each of its L strongest interferers and itself.

1) *Spatial Interference Cancellation and Opportunistic Transmission:* The idea of spatial interference cancellation is to apply zero-forcing beamforming at R_0 for canceling interference from strong interferers. The details of the interference cancellation algorithm are provided as follows.

Let \mathbf{f}_n and \mathbf{v}_0 denote the transmit beamformer at T_n and the receive beamformer at R_0 , respectively. From the perspective of R_0 , the interference channel from T_n ($n \neq 0$) appears as an effective channel vector $\mathbf{h}_n = \mathbf{H}_n \mathbf{f}_n$, where \mathbf{H}_n denotes the actual MIMO channel. To facilitate our discussion, the indices of the transmitting nodes interfering with R_0 are sorted according to their effective interference channel norms, namely $\|\mathbf{h}_1\| \geq \|\mathbf{h}_2\| \geq \dots \geq \|\mathbf{h}_L\| \dots$. The crux of the interference cancellation algorithm is to constrain the beamforming vector \mathbf{v}_0 of R_0 to be in the null space of the matrix $[\mathbf{h}_1, \mathbf{h}_2, \dots, \mathbf{h}_{L-1}]$. Thereby, the interference from $(L - 1)$ strongest interferers to R_0 is nulled⁵: $|\mathbf{v}_0^\dagger \mathbf{h}_1| = |\mathbf{v}_0^\dagger \mathbf{h}_2| \dots = |\mathbf{v}_0^\dagger \mathbf{h}_{L-1}| = 0$, where \dagger represents the complex conjugate and transpose matrix operation. Note that

⁵With probability one, the matrix $[\mathbf{h}_1, \mathbf{h}_2, \dots, \mathbf{h}_{L-1}]$ has full rank. Thus, with L antennas, R_0 can cancel at most $(L - 1)$ interferers.

perfect CSI estimation of $\mathbf{h}_1, \mathbf{h}_2, \dots, \mathbf{h}_{L-1}$ by R_0 is required to completely cancel the interference from $(L-1)$ strongest interferers. CSI estimation at each receiver uses pilot symbols broadcast by transmitters. The issue of CSI inaccuracy is addressed in Section III-B.

An arbitrary transmit beamformer is applied at T_0 , represented by \mathbf{f}_0 . Without performing interference pre-cancellation, T_0 need not acquire CSI of the channels linking T_0 and the interfered receivers, which is difficult. Note that an attempt to perform *maximum ratio transmission* [43] causes iterative updating of beamforming vectors at all nodes and potential network instability. By such beamforming, multiple transmit antennas contribute no diversity gain, but they are needed for interference cancellation when the transmitter becomes a receiver.

To avoid deep fading due to the lack of diversity gain, opportunistic transmission is applied. Consequently, transmission at each transmitter is turned on only if the channel gain $S = |\mathbf{v}_0^\dagger \mathbf{H}_0 \mathbf{f}_0|^2$ is above a threshold denoted by $\beta_0 = \beta d^{-\alpha}$, where β is an equivalent threshold applied on the fading gain. It follows that the random-access probability for each potential transmitter is $P_t = \Pr(S \geq \beta d^{-\alpha})$ (cf. Section II-A). This algorithm is also used in [1] for single-antenna ad hoc networks and similar concepts exist in optimal power control for fading channels [44], [45]. The threshold β should be sufficiently small so as not to cause excessive delay before transmission.⁶

2) *Effective Channel and Network Models*: The following effective channel and network models result from the application of the interference cancellation algorithm in the preceding section.

With perfect interference cancellation, R_0 receives interference only from the nodes⁷ $\{T_n \mid n \geq L\}$. Recall that r_n and I_n denote respectively the distance between T_n and the origin, and the interference power from T_n to R_0 . Based on the channel model in Section II-B, for $n \geq L$, the effective interference power $I_n = P_D |\mathbf{v}_0^\dagger \mathbf{H}_n \mathbf{f}_n|^2 = r_n^{-\alpha} |\mathbf{v}_0^\dagger \mathbf{G}_n \mathbf{f}_n|^2$. Let $\rho_n = |\mathbf{v}_0^\dagger \mathbf{G}_n \mathbf{f}_n|^2$, so that for $n \geq L$, $I_n = r_n^{-\alpha} \rho_n$. Because both \mathbf{f}_n and \mathbf{v}_0 are independent⁸ of \mathbf{G}_n and \mathbf{G}_n is an i.i.d. complex Gaussian matrix, the random variable ρ_n will have an exponential distribution with unit mean.

The effective power of the data link from T_0 to R_0 is given by $S = |\mathbf{v}_0^\dagger \mathbf{H}_0 \mathbf{f}_0|^2 = d^{-\alpha} |\mathbf{v}_0^\dagger \mathbf{G}_0 \mathbf{f}_0|^2$ with $S \geq \beta d^{-\alpha}$ due to opportunistic transmission. Recall that d is the distance between T_0 and R_0 , $\beta d^{-\alpha}$ is the transmission threshold, and \mathbf{G}_0 is the fading component of the MIMO channel \mathbf{H}_0 . Because the beamformers \mathbf{v}_0 and \mathbf{f}_0 are independent of \mathbf{G}_0 as discussed in the preceding section, the random variable

⁶Implementing this opportunistic scheme requires some form of hand-shaking between the transmitter and receiver and limited coordination among neighboring nodes. In particular, note that the transmission decision depends on the chosen value of \mathbf{v}_0 , which in turn depends on the transmission decisions of the neighboring transmitters. We leave the development of such a protocol for future work.

⁷Note that the indices of the nodes $\{T_n\}$ are sorted according to the power of their interference to R_0 .

⁸Note that the interference canceling beamformer \mathbf{v}_0 is a function of $\{\mathbf{G}_n \mid 1 \leq n \leq L-1\}$ but independent of $\{\mathbf{G}_n \mid n \geq L\}$. Moreover, the transmit beamformer \mathbf{f}_n is random and hence independent of any interference channel.

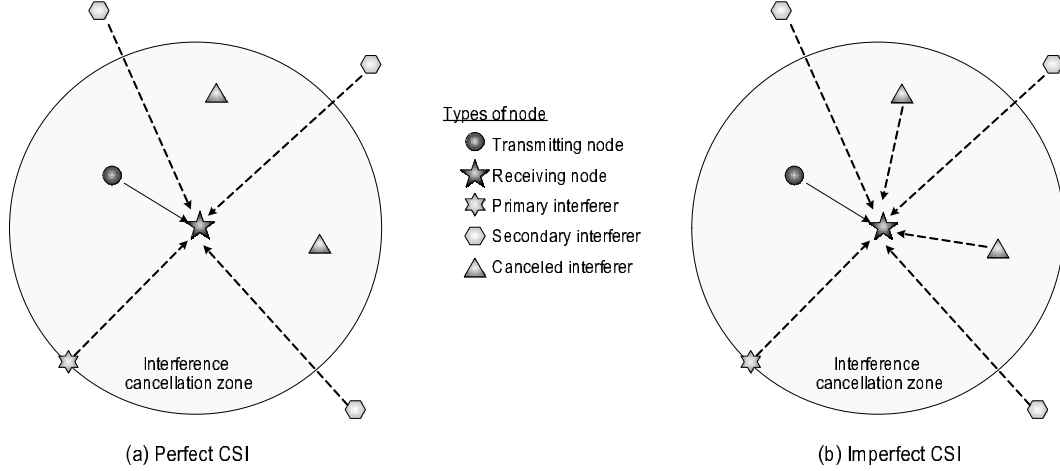


Fig. 1. Effective channel and network models resulting from interference cancellation with (a) perfect CSI or (b) imperfect CSI for antenna arrays of three elements. The distance in the figures is proportional to the effective channel power. The data and interference links are plotted by using solid and dashed lines, respectively.

$W = |\mathbf{v}_0^\dagger \mathbf{G}_0 \mathbf{f}_0|^2$ has the exponential distribution with the following probability density function

$$f_W(w) = \exp(-w)/P_t, \quad w \geq \beta \quad (4)$$

where $P_t = \exp(-\beta)$.

Last, the effective channel and network models resulting from interference cancellation is illustrated in Fig. 1(a). Note that the density of transmitting nodes is $\lambda = P_t \lambda_o$. Based on the above models, the SIR at R_0 is given as

$$\text{(Perfect CSI)} \quad \text{SIR} = \frac{d^{-\alpha} W}{\sum_{n=L}^{\infty} r_n^{-\alpha} \rho_n}. \quad (5)$$

B. Imperfect CSI

1) *CSI Estimation*: As discussed in Section III, interference cancellation at R_0 requires the estimation of CSI on the effective channels vectors corresponding to the $(L - 1)$ strongest interferers of R_0 . The CSI estimation is facilitated by the transmission of pilot symbols from these interferers. Let M denote the length of the pilot sequence sent by each interferer. The $(L - 1)$ pilot sequences form the columns of a $(L - 1) \times M$ matrix, represented by \mathbf{Q} , where $M \geq (L - 1)$. Following [46], \mathbf{Q} is designed as a unitary matrix. A protocol for CSI estimation may consist of two phases, where a receiver first identifies the $(L - 1)$ strongest interferers by estimating their interference power and then estimates CSI for canceling these interferers. Given the unitary constraint for \mathbf{Q} , this protocol should allow a transmitter to send different CSI training sequences to different receivers.⁹ The detailed design of the CSI estimation

⁹Removing the unitary constraint for \mathbf{Q} simplifies the CSI estimation protocol as a transmitter can broadcast the same training sequence to all receivers. Nevertheless, allowing the columns of \mathbf{Q} to be non-orthogonal potentially introduces coupling between the estimated CSI for different interferers and complicates CSI estimation as well as analysis.

protocol will be addressed in future work.

The CSI training signal received at R_0 , denoted as \mathbf{y} , is given as

$$\mathbf{y}^T = \sqrt{M} [\mathbf{h}_1, \mathbf{h}_2, \dots, \mathbf{h}_{L-1}] \mathbf{Q} + \sum_{n=L}^{\infty} \mathbf{h}_n \mathbf{x}_n^T \quad (6)$$

where \sqrt{M} ensures the transmission power of each node that sends pilot symbols is $P_D = 1$, and the $M \times 1$ vector \mathbf{x}_n contains $\mathcal{CN}(0, 1)$ data symbols transmitted by the n th transmitter. The summation term in (6) represents interference to the CSI estimation at R_0 . The CSI, denoted as $\hat{\mathbf{h}}_1, \hat{\mathbf{h}}_2, \dots, \hat{\mathbf{h}}_{L-1}$, is estimated using the least-square method, thus

$$[\hat{\mathbf{h}}_1, \hat{\mathbf{h}}_2, \dots, \hat{\mathbf{h}}_{L-1}] = \frac{1}{\sqrt{M}} \mathbf{y}^T \mathbf{Q}^\dagger = [\mathbf{h}_1, \mathbf{h}_2, \dots, \mathbf{h}_{L-1}] + \frac{1}{\sqrt{M}} \sum_{n=L}^{\infty} \mathbf{h}_n \tilde{\mathbf{x}}_n^T \quad (7)$$

where $\tilde{\mathbf{x}}_n^T = \mathbf{x}_n^T \mathbf{Q}^\dagger$ is a $1 \times (L-1)$ i.i.d. $\mathcal{CN}(0, 1)$ vector. Note that the alternative MMSE method requires estimating the covariance of the aggregate interference from the transmitters T_L, T_{L+1}, \dots . Such estimation is potentially inaccurate due to the presence of the strong interferers T_1, T_2, \dots, T_{L-1} . It follows from (7) that

$$\mathbf{h}_l = \hat{\mathbf{h}}_l - \frac{1}{\sqrt{M}} \sum_{n=L}^{\infty} \mathbf{h}_n \tilde{x}_{n,l}, \quad l = 1, 2, \dots, L-1. \quad (8)$$

The estimated CSI is applied for computing the beamforming vector \mathbf{v}_0 used at R_0 under the zero-forcing constraint $\mathbf{v}_0 \perp [\hat{\mathbf{h}}_1, \hat{\mathbf{h}}_2, \dots, \hat{\mathbf{h}}_{L-1}]$. Thus, using (8), the residual interference at R_0 after beamforming, denoted as I_r , can be written as

$$I_r = \sum_{l=1}^{L-1} \mathbf{v}_0^\dagger \mathbf{h}_l x_l = -\frac{1}{\sqrt{M}} \sum_{l=1}^{L-1} \sum_{n=L}^{\infty} r_n^{-\alpha/2} a_n \tilde{x}_{n,l} x_l$$

where $a_n = r_n^{\alpha/2} \mathbf{v}_0^\dagger \mathbf{h}_n$ is $\mathcal{CN}(0, 1)$ since \mathbf{v}_0 and \mathbf{h}_n are independent. Therefore, I_r is $\mathcal{CN}(0, \sigma_r^2)$ with the variance σ_r^2 given as

$$\sigma_r^2 = \frac{1}{M} \sum_{l=1}^{L-1} \left| \sum_{n=L}^{\infty} r_n^{-\alpha/2} a_n \tilde{x}_{n,l} \right|^2. \quad (9)$$

2) *Effective Channel and Network Models:* As illustrated in Fig. 1(b), the effective channel and network models for interference cancellation with imperfect CSI is identical to that for the case of perfect CSI except for the additional residual interference from the nodes $\{T_n \mid 1 \leq n \leq L-1\}$. For the present case, the SIR in (5) is modified as

$$(\text{Imperfect CSI}) \quad \widetilde{\text{SIR}} = \frac{d^{-\alpha} W}{\sigma_r^2 + \sum_{n=L}^{\infty} r_n^{-\alpha} \rho_n}. \quad (10)$$

It is worth mentioning that the present model of residual interference is more accurate than that in [7] for SIC with imperfect CSI. In [7], the residual interference power is modeled as $z \sum_{n=1}^L r_n^{-\alpha}$ where the parameter $0 \leq z \leq 1$ controls the degree of CSI accuracy. The overhead and algorithm for CSI estimation considered in the present model are not accounted for in [7].

IV. OUTAGE PROBABILITY AND TRANSMISSION CAPACITY: PERFECT CSI

This section focuses on the analysis of the outage probability for a SIR constraint and the network transmission capacity for perfect CSI. In particular, the scaling law of transmission capacity is derived for the regime of small outage probability.

A. Auxiliary Results

To facilitate analysis, the interfering nodes of R_0 after perfect interference cancellation, namely $\{T_n \mid n \geq L\}$, are separated into the strongest interferer T_L and the remaining interferers $\{T_n \mid n \geq L+1\}$, referred to respectively as the *primary* and the *secondary* interferers. For convenience, denote the random interference power from T_L as $G = I_L$. There are two reasons for the above separation of the interferers. First, considering the strongest interferer T_L alone yields a lower bound for the outage probability to be derived in the next section. Second, the separation of interferers provides a useful result that conditioning on G , the secondary interferers $\{T_n \mid n \geq L+1\}$ form a Poisson point process as shown shortly.

The result stated above is obtained by using the Marking Theorem [38]. To apply this theorem, a *marked point process* is defined for the secondary interferers, where the mark of the node T_n is the corresponding interference power I_n . Specifically, conditioning on the interference power of the primary interferer $G = g$, the desired marked point process is

$$\Pi(g) = \{(T_n, I_n) \mid T_n \in \Phi \setminus \{T_0\}, 0 \leq I_n < g\} \quad (11)$$

where Φ is the homogeneous Poisson point process modeling all active transmitters (cf. Section II-A). Note that conditioning on $G = g$, the marks $\{I_n\}$ are independent. Given this condition, the result in the following lemma directly follows from the Marking Theorem [38].

Lemma 1: The process $\Pi(g)$ is a homogeneous Poisson point process on $\mathbb{R}^2 \times \mathbb{R}^+$ with the average number of nodes given by

$$\mu(g) = 2\pi\lambda \int_0^\infty \int_0^g r p(r, dI) dr \quad (12)$$

where $p(r, \cdot)$ is the distribution function of I_n conditioned on $d_n = r$.

This result is useful for analyzing the aggregate interference from the secondary interferers to R_0 . Conditioned on $G = g$, this interference is written as

$$I_\Pi(g) = \sum_{(T_n, I_n) \in \Pi(g)} I_n. \quad (13)$$

The process $I_\Pi(g)$ in (13) is known as a *shot noise process* [38]. The probability density function of $I_\Pi(g)$ is difficult to derive and has no closed-form expression except for some simple cases [1], [37]. Nevertheless, using the Marking theorem, the first and second moments of this process are characterized in the following lemma.

Lemma 2: After perfect interference cancellation, the interference at R_0 has the following properties.

- (a) The interference power of the primary interferer G has the following probability density function

$$f_G(g) = \frac{\delta \nu^L \lambda^L}{\Gamma(L)} g^{-\delta L - 1} \exp(-\nu \lambda g^{-\delta}) \quad (14)$$

where $\delta := \frac{2}{\alpha}$ and $\nu := \pi \Gamma(1 + \delta)$.

- (b) Conditioned on $G = g$, the mean and variance of the aggregate interference power from the secondary interferers are given by

$$\mathbf{E}[I_\Pi(g)] = \frac{\delta \nu \lambda}{1 - \delta} g^{1-\delta} \quad (15)$$

$$\text{Var}(I_\Pi(g)) = \frac{2\delta \nu \lambda}{2 - \delta} g^{2-\delta}. \quad (16)$$

Proof: See Appendix A. \square

B. Bounds on Outage Probability

From (5) and the separation of interferers in the preceding section, the outage probability P_{out} can be written as

$$P_{\text{out}}(\lambda) = \Pr(\text{SIR} \leq \theta) = \mathbf{E}[\Pr(I_\Pi(g) \geq w\psi - g \mid G, W)] \quad (17)$$

where $\psi := \theta^{-1}d^{-\alpha}$, W is the fading component of the data link power for R_0 (cf. Section III-A.2), G and $I_\Pi(g)$ are respectively the interference power of the *primary* and *secondary* interferers. The direct analysis of the exact outage probability by using (17) is infeasible due to the difficulty in deriving the distribution function of $I_\Pi(g)$. Instead, we bound P_{out} , following the approaches in [1], [2], [7].

The expression of the outage probability in (17) can be rewritten as

$$P_{\text{out}}(\lambda) = \Pr(G \geq W\psi) + \mathbf{E}[\Pr(I_\Pi(g) \geq w\psi - g \mid G < W\psi)] \Pr(G < W\psi). \quad (18)$$

Thus, a lower bound of P_{out} is given as

$$P_{\text{out}}(\lambda) \geq \Pr(G \geq W\psi). \quad (19)$$

This lower bound considers only the primary interference, and hence is nearly tight if the primary interferer T_L is the dominant source of interference. Next, an upper bound on the outage probability can be derived by applying the following Chebyshev's inequality on (18)

$$\Pr(I_\Pi(g) \geq a) \leq \min \left\{ \frac{\text{Var}(I_\Pi(g))}{\{a - \mathbf{E}[I_\Pi(g)]\}^2}, 1 \right\}, \quad \forall a > \mathbf{E}[I_\Pi(g)]. \quad (20)$$

Based on (18), (19) and (20), bounds on the outage probability are derived as shown in the following theorem.

Theorem 1: For perfect CSI, the bounds on the outage probability are given as follows.

1) The lower bound is

$$P_{\text{out}}^l(\lambda) = \frac{\gamma(L, \nu\psi^{-\delta}\beta^{-\delta}\lambda)}{\Gamma(L)} - \frac{\delta(\nu\psi^{-\delta})^L\lambda^L}{\Gamma(L)P_t} \int_{\beta}^{\infty} g^{-\delta L-1} \exp(-\nu\psi^{-\delta}\lambda g^{-\delta} - g) dg.$$

2) Define the sets $\mathcal{D}_1 = \{(w, g) \mid 0 \leq g < g_0, w \geq \beta\}$ and $\mathcal{D}_2 = \{(w, g) \mid g \geq g_0, w \geq g + \mathbf{E}[I_{\Pi}(g)]\}$.

Moreover, let g_0 denote a constant that satisfies the equation $g_0 + \mathbf{E}[I_{\Pi}(g_0)] = \beta\psi$, where $\mathbf{E}[I_{\Pi}(g)]$ is given in Lemma 2. The upper bound on the outage probability is

$$P_{\text{out}}^u(\lambda) = \iint_{(w,g) \in \mathcal{D}_1 \cup \mathcal{D}_2} \min\left(\frac{\frac{\delta\nu}{2-\delta}\lambda g^{2-\delta}}{(w\psi - g - \frac{\delta\nu}{1-\delta}\lambda g^{1-\delta})^2}, 1\right) f_W(w)f_G(g)dw dg + P_{\alpha}(\lambda) \quad (21)$$

where

$$P_{\alpha}(\lambda) = \frac{\gamma(L, \nu g_0^{-\delta}\lambda)}{\Gamma(L)} - \frac{\delta\nu^L\lambda^L}{P_t\Gamma(L)} \int_{g_0}^{\infty} g^{-\delta L-1} \exp\left(-\psi^{-1}g - \frac{\delta\nu}{1-\delta}\psi^{-1}\lambda g^{1-\delta} - \nu\lambda g^{-\delta}\right) dg$$

and $\gamma(\cdot, \cdot)$ denotes the incomplete Gamma function.

Proof: See Appendix B. □

The above bounds on P_{out} do not provide simple closed-form expressions in terms of the node density λ . The difficulty in deriving such closed-form expressions is mainly due to the existence of multiple random variables, namely W , G and $I_{\Pi}(G)$, which jointly determine the outage probability. The tightness of the above bounds on P_{out} is evaluated using simulation in Section VI.

C. Asymptotic Transmission Capacity

In this section, the scaling law for transmission capacity is derived for small target outage probability ($\epsilon \rightarrow 0$) and perfect CSI. This scaling law also accurately characterizes transmission capacity in the non-asymptotic outage regime (up to 0.1) as shown by simulations in Section VI.

Small target outage probability results in a network of sparse transmitting nodes (i.e. $\lambda \rightarrow 0$). For such a sparse network, the useful relationship between the outage probability and node density is given in the following lemma.

Lemma 3: For perfect CSI and $\lambda \rightarrow 0$, the outage probability scales with λ as follows.

1) For $L \leq \alpha$,

$$\kappa_1 \leq \lim_{\lambda \rightarrow 0} \frac{P_{\text{out}}(\lambda)}{\lambda^L} \leq \kappa_2 \quad (22)$$

$$\text{where } \kappa_1 = \frac{\Gamma(1-\delta L, \beta)(\nu\theta^{\delta}d^2)^L}{P_t\Gamma(L+1)} \text{ and } \kappa_2 = \kappa_1 \left[1 + 2^{\delta L}L \left(\frac{2}{2-\delta} - 2^{-\delta}\right)\right].$$

2) For $L > \alpha$,

$$\kappa_1 \leq \lim_{\lambda \rightarrow 0} \frac{P_{\text{out}}(\lambda)}{\lambda^L}, \quad \lim_{\lambda \rightarrow 0} \frac{P_{\text{out}}(\lambda)}{\lambda^{\alpha}} \leq \kappa_3 \quad (23)$$

$$\text{where } \kappa_3 = \frac{4\delta\psi^{-2}\nu^{\alpha}\Gamma(-1, \beta)\Gamma(L-\alpha+1)}{(2-\delta)\Gamma(L)}.$$

Proof: See Appendix C. □

Note that the ratio $\frac{\kappa_2}{\kappa_1}$ decreases as L reduces. This suggests that the asymptotic bounds are tighter for smaller values of L .

Using Lemma 3 and the definition of transmission capacity in (3), the main result of this section is obtained and summarized in the following theorem.

Theorem 2: For perfect CSI and small target outage probability $\epsilon \rightarrow 0$, the transmission capacity scales as

1) For $L \leq \alpha$,

$$\lim_{\epsilon \rightarrow 0} \frac{C(\epsilon)}{\kappa_2^{-\frac{1}{L}} \epsilon^{\frac{1}{L}}} \geq 1, \quad \lim_{\epsilon \rightarrow 0} \frac{C(\epsilon)}{\kappa_1^{-\frac{1}{L}} \epsilon^{\frac{1}{L}}} \leq 1 \quad (24)$$

where κ_1 and κ_2 are specified in Lemma 3.

2) For $L > \alpha$,

$$\lim_{\epsilon \rightarrow 0} \frac{C(\epsilon)}{\kappa_3^{-\frac{1}{\alpha}} \epsilon^{\frac{1}{\alpha}}} \geq 1, \quad \lim_{\epsilon \rightarrow 0} \frac{C(\epsilon)}{\kappa_1^{-\frac{1}{L}} \epsilon^{\frac{1}{L}}} \leq 1 \quad (25)$$

where κ_3 is given in Lemma 3.

The above theorem shows that as the target outage probability decreases, transmission capacity grows following the power law $a\epsilon^t$ where a and t are constants. For $L > \alpha$, only bounds on the exponent t are known. We conjecture that for $L > \alpha$, $t = 1/L$. In other words, the exact scaling law is within a multiplicative factor of the asymptotic lower bound in the above theorem, which is confirmed by simulation results (cf. Fig. 5(b)). The derivation of the exact scaling law for $L > \alpha$ requires a tighter upper bound on outage probability than that based on Chebyshev's inequality in (20). This may require analyzing the distribution function of the secondary interference power (cf. Section III-A.2), which, however, has no closed-form expression for the present case [47].

For $L \leq \alpha$, the exponent of the transmission capacity power law $a\epsilon^t$ is shown in Theorem 2 to be $t = 1/L$, and α is bounded as $\kappa_2^{-\frac{1}{L}} \leq \alpha \leq \kappa_1^{-\frac{1}{L}}$. This power law indicates that the size of antenna array L determines the sensitivity of transmission capacity to the change on the outage constraint. To facilitate our discussion, rewrite the scaling law in Theorem 2 as $C(\epsilon) \cong \alpha \epsilon^{\frac{1}{L}}$ where “ \cong ” represents asymptotic equivalence for $\epsilon \rightarrow 0$. Moreover, consider two sets of values (C_1, ϵ_1) and (C_2, ϵ_2) , and define the logarithmic ratios $\Delta C = \log \frac{C_1}{C_2}$ and $\Delta \epsilon = \log \frac{\epsilon_1}{\epsilon_2}$. Using this notation, the above scaling law can be written as

$$\frac{\Delta C}{\Delta \epsilon} \cong \frac{1}{L}. \quad (26)$$

The above quantity $\frac{\Delta C}{\Delta \epsilon}$ represents the sensitivity of transmission capacity towards changes in the outage constraint. Its value decreases inversely with the size of antenna array. Specifically, computed using (26), a hundred-time decrease on ϵ reduces network transmission capacity by $\{10, 3.2, 1.8\}$ times for $L = \{2, 4, 8\}$, respectively. For the extreme case of $L = \infty$, transmission capacity is independent of the outage constraint since $\frac{\Delta C}{\Delta \epsilon} = 0$. Last, from simulation results in Section VI, the capacity scaling law in Theorem 2 is observed to also hold in the outage regime of practical interest ($\epsilon \leq 0.1$).

V. OUTAGE PROBABILITY AND TRANSMISSION CAPACITY: IMPERFECT CSI

In this section, the SIR outage probability and transmission capacity are analyzed for the case of imperfect CSI.

From (10), the SIR outage probability for the case of imperfect CSI is written as

$$\tilde{P}_{\text{out}}(\lambda) = \Pr \left(\frac{Wd^{-\alpha}}{\sigma_r^2 + \sum_{l=1}^{L-1} r_n^{-\alpha} \rho_n} \leq \theta \right) \quad (27)$$

where σ_r^2 is the power of the residual interference given in (9). This probability is related to that for the case of perfect CSI in the following theorem.

Theorem 3: For the case of imperfect CSI, the SIR outage probability is bounded as

$$P_{\text{out}}(\lambda) \leq \tilde{P}_{\text{out}}(M, \lambda) \leq P_{\text{out}}(\lambda) \left(1 + \frac{Z}{M} \right) + 2^{L-1} e^{-\omega Z}, \quad M \geq L - 1 \quad (28)$$

where P_{out} is the outage probability given perfect CSI, $Z > 0$ is arbitrary and $\omega = [\Gamma(L)]^{-\frac{1}{L-1}}$.

Proof: See Appendix D. □

The result in Theorem 3 can be interpreted using two corollaries. The following corollary is obtained by setting $Z = M^q$ in (28) with $q \in (0, 1)$ and $M \rightarrow \infty$, and then let $q \rightarrow 0$.

Corollary 1: For $M \rightarrow \infty$ and fixed λ , the outage probability given imperfect CSI converges to that for perfect CSI as follows

$$\frac{\tilde{P}_{\text{out}}(M, \lambda)}{P_{\text{out}}(\lambda)} = 1 + O \left(\frac{1}{M} \right). \quad (29)$$

This corollary agrees with the intuition that increasing the amount of CSI training overhead reduces the effect of CSI inaccuracy. Moreover, (29) shows that the effect of imperfect CSI disappears at a rate proportional to the inverse of the pilot sequence length. The next corollary of Theorem 3 characterizes how much CSI training overhead is needed for containing the effect of CSI inaccuracy.

Corollary 2: To ensure $\tilde{P}_{\text{out}}(M, \lambda) \leq (1 + \xi) P_{\text{out}}(\lambda)$ with $\xi > 0$, it is sufficient to choose the length of the CSI training sequence as

$$M = \max \left(\left\lceil \frac{2}{\xi \omega} (L \log 2 - \log P_{\text{out}}(\lambda) - \log \xi) \right\rceil, L - 1 \right). \quad (30)$$

where $\lceil a \rceil$ gives the smallest integer larger than a .

This corollary is derived by substituting $Z = -\frac{1}{\omega} \log(2^{-L} P_{\text{out}} \xi)$ and $M = 2Z/\xi$ into (28), and taking into account that $M \geq L - 1$ and M is an integer. The result in Corollary 2 shows that for given ξ , M increases linearly with L and logarithmically with the inverse of P_{out} .

Finally, the required length of pilot sequence is derived for achieving the scaling laws of transmission capacity close to those for the case of perfect CSI. Define the transmission capacity for imperfect CSI as $\tilde{C}(M, \epsilon) = (1 - \epsilon) \tilde{P}_{\text{out}}^{-1}(M, \epsilon)$. The scaling laws of $\tilde{C}(M, \epsilon)$ are given in the following theorem.

Theorem 4: For $0 < \varphi < 1$, choosing the length of pilot sequence for CSI estimation as $M_\epsilon(\varphi) = \max\left(\left\lceil \tilde{M}(\varphi) \right\rceil, L - 1\right)$ with

$$\tilde{M}(\varphi) = \begin{cases} \frac{\varphi^L}{(1 - \varphi^L)\omega} [(L - 1) \log 2 - 2 \log \epsilon], & L \leq \alpha \\ \frac{\varphi^\alpha}{(1 - \varphi^\alpha)\omega} [(\alpha - 1) \log 2 - 2 \log \epsilon], & L > \alpha \end{cases} \quad (31)$$

achieves the scaling laws of transmission capacity for a small target outage probability ($\epsilon \rightarrow 0$) given as

1) For $L \leq \alpha$:

$$\lim_{\epsilon \rightarrow 0} \frac{\tilde{C}(M_\epsilon, \epsilon)}{\kappa_2^{-\frac{1}{L}} \epsilon^{\frac{1}{L}}} \geq \varphi, \quad \lim_{\epsilon \rightarrow 0} \frac{\tilde{C}(M_\epsilon, \epsilon)}{\kappa_1^{-\frac{1}{L}} \epsilon^{\frac{1}{L}}} \leq 1$$

2) For $L > \alpha$:

$$\lim_{\epsilon \rightarrow 0} \frac{\tilde{C}(M_\epsilon, \epsilon)}{\kappa_3^{-\frac{1}{\alpha}} \epsilon^{\frac{1}{\alpha}}} \geq \varphi, \quad \lim_{\epsilon \rightarrow 0} \frac{\tilde{C}(M_\epsilon, \epsilon)}{\kappa_1^{-\frac{1}{L}} \epsilon^{\frac{1}{L}}} \leq 1$$

where κ_1 , κ_2 , and κ_3 are given in Lemma 3.

Proof: See Appendix E. □

Theorem (4) shows that CSI inaccuracy introduces only an additional linear throughput scaling factor, namely $0 < \varphi < 1$, without affecting the exponents in the throughput scaling laws. As shown by Fig. 2, the required length of pilot sequence M_ϵ increases relatively gradually with growing φ in the regime of $0 < \varphi < 0.6$ but very rapidly in the regime $0.6 < \varphi < 1$. In the regime of small φ , M_ϵ grows as L increases due to the constraint that $M \geq L - 1$. Nevertheless, the reverse holds in the large φ regime. The reason is that increasing L reduces the number of strong interferers for CSI estimation at each receiver, and hence requires less CSI overhead.

VI. SIMULATION AND DISCUSSION

In this section, the bounds on outage probability and the network transmission capacity are evaluated using Monte Carlo simulation. The procedure for simulating a MANET follows that in [48]. The simulated ad hoc network lies on a two-dimensional disk and contains a number of transmitter-receiver pairs, which follows the Poisson distribution with the mean equal to 200. The locations of the nodes are uniformly distributed on the disk. The disk area is adjusted according to the node density. The typical receiver is placed at the center of the disk. We set the distance between the typical transmitter and receiver as $d = 5$ m, the required SIR as $\theta = 3$ or 4.8 dB, the transmission threshold $\beta = 1$, and the path-loss exponent as $\alpha = 4$.

A. Bounds on Outage Probability

For perfect CSI, the bounds on outage probability from Theorem 1 and simulated values are compared in Fig. 3. The number of antenna per node is $L = \{2, 4\}$. As observed from Fig. 3, the bounds for $L = 2$

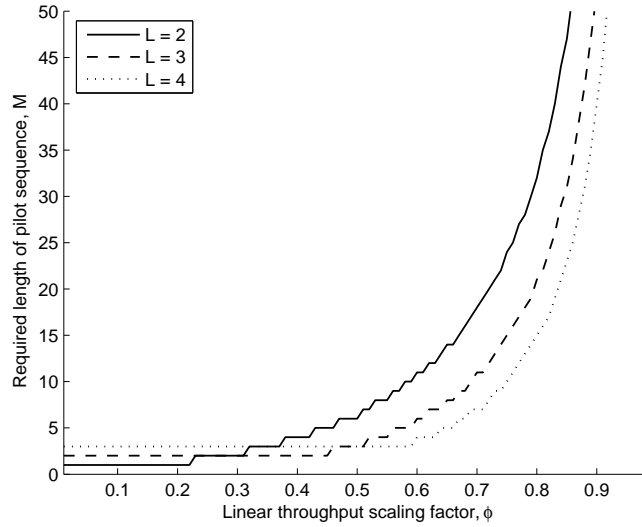


Fig. 2. For imperfect CSI, the required length of pilot sequence M_ϵ vs. the increasing throughput scaling factor φ for $L = \{2, 3, 4\}$ and $\epsilon = 0.01$.

are tighter than those for $L = 4$. Moreover, the bounds and the simulated values of the outage probability converge as the transmitting node density λ decreases. These two observations can be explained by the dominance of the primary interference over the secondary one as L increases or λ decreases, where the secondary interference causes the looseness of the bounds on outage probability. Finally, the outage probability is approximately proportional to λ^L .

In Fig. 4, the SIR outage probability for imperfect CSI is evaluated against that for perfect CSI, where the transmitting node density is varied and different lengths of pilot sequence are considered. The number of antennas per node is $L = 4$. The length of pilot sequence is fixed at $M = \{3, 5, 11\}$ in Fig. 4(a) but varied with the node density in Fig. 4(b) based on Corollary 2. As observed from Fig. 4(a), increasing M rapidly converges the outage probability for imperfect CSI to its lower bound corresponding to perfect CSI. In particular, for $M = 11$, CSI inaccuracy increases outage probability by less than a factor of two. In Fig. 4(a), M varies with the node density according to (30) with $\xi = \{1, 5\}$. Regardless of the node density, the outage probability for imperfect CSI is bounded within $(1 + \xi)$ times its lower bound, which validates Corollary 2. For instance, the ratio between the outage probabilities for imperfect and perfect CSI is about 3 with is smaller then the upper-bound $(1 + \xi) = 5$ given in Corollary 2.

B. Scaling Laws of Transmission Capacity

In Fig. 5, asymptotic bounds on transmission capacity in Theorem 2 are compared with the exact values obtained by simulation for perfect CSI and the range of target outage probability $\epsilon \in [10^{-5}, 0.1]$. The corresponding curves are identified using the legends “asymptotic upper bound”, “asymptotic lower

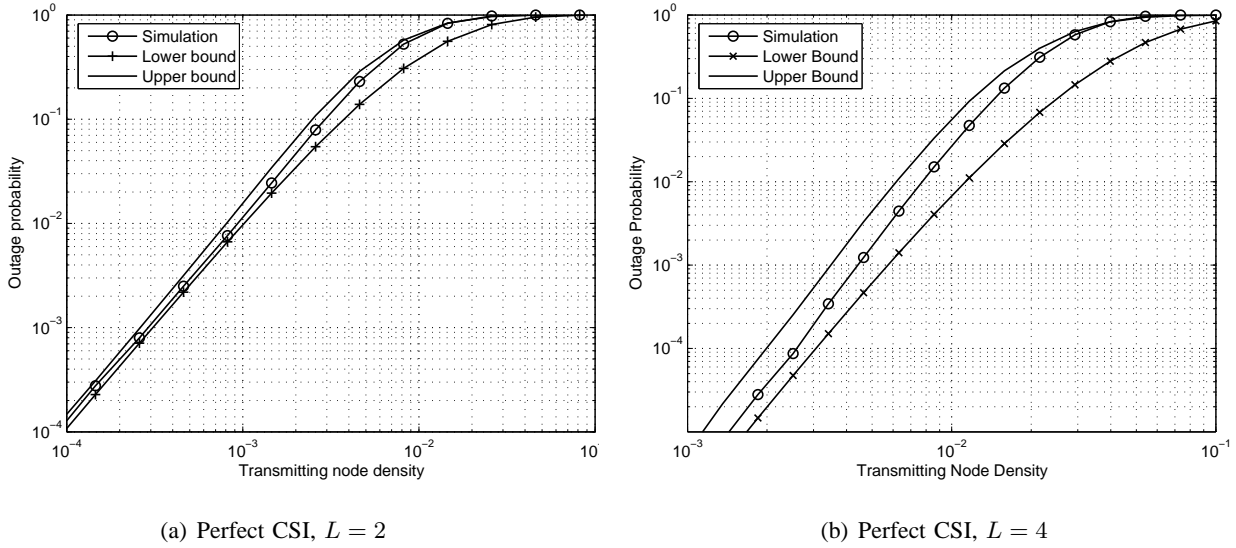


Fig. 3. Outage probability for different transmitting node densities and perfect CSI. The size of the antenna array is (a) $L = 2$ and (b) $L = 4$.

bound”, and “simulation”. Different combinations of $L = \{2, 4, 5\}$ and $\alpha = \{3, 4\}$ are separated according to the cases of $L \leq \alpha$ and $L > \alpha$, corresponding to Fig. 5(a) and Fig. 5(b), respectively. As observed from Fig. 5(a), for $L \leq \alpha$, the asymptotic upper bound on transmission capacity is tight even in the non-asymptotic range e.g. $\epsilon \in [0.01, 0.1]$. The tightness of this bound is due to the dominance of primary interference for interference cancellation with small sizes of antenna array. Moreover, Fig. 5(b) shows that for $L > \alpha$ the slopes of the “simulation” curves converge to those of the corresponding “asymptotic upper bound” curves as the target outage probability decreases. The above observations suggest that for both $L \leq \alpha$ and $L > \alpha$, the scaling laws of transmission capacity for small target outage probabilities follow the power laws with the same exponent equal to $1/L$.

C. Transmission Capacity vs. Size of Antenna Array

In Fig. 6, the transmission capacity is plotted for an increasing number of antennas per node assuming perfect CSI. Furthermore, different outage constraints, namely $\epsilon = \{10^{-1}, 10^{-2}, 10^{-3}\}$, are considered. From Fig. 6, the following observations are made. First, the use of multiple antennas for interference cancellation leads to the increase in transmission capacity by an order of magnitude or more with respect to the case of single-antenna per node. This capacity gain is especially large for a small number of antennas and small target outage probability. For example, for $\epsilon = 10^{-1}$, the use of three antennas per node provides transmission capacity seven times of that for the single-antenna case. The capacity gain by using additional antennas diminishes rapidly as the number of antennas per node increases. Second, the outage constraint affects transmission capacity significantly for a small number of antennas per node. Nevertheless, transmission capacity becomes insensitive to changes in the outage constraint as the number

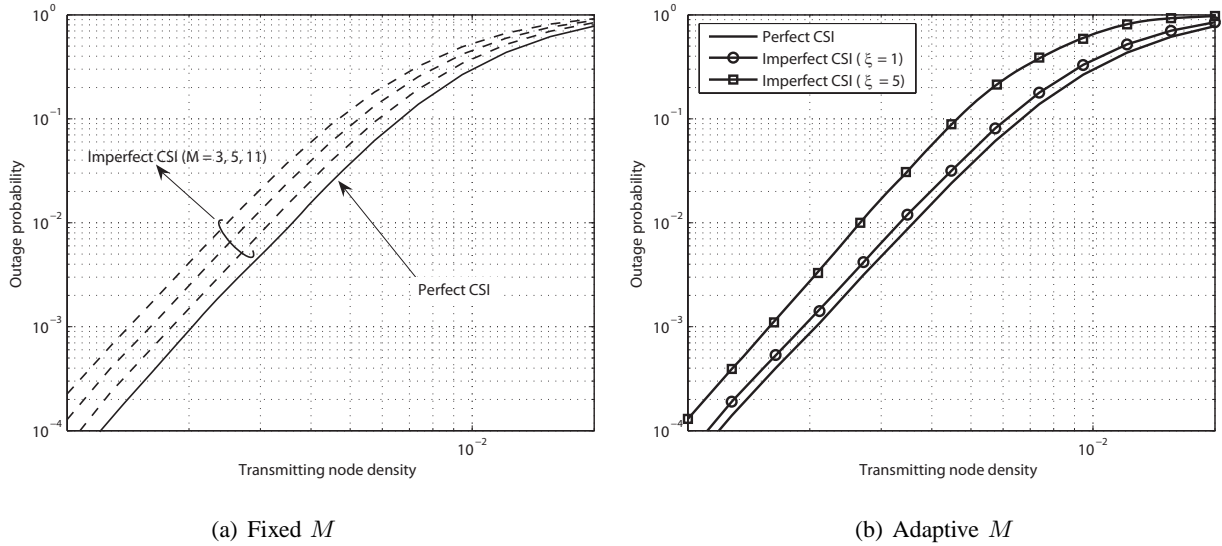


Fig. 4. Compare outage probability for perfect and imperfect CSI given different transmitting node densities. The length of pilot sequence is (a) fixed at $M = \{3, 5, 11\}$ or (b) adapted to the node density according to (30) for $\xi = \{1, 5\}$. The size of the antenna array is $L = 4$.

of antennas increases.

The effect of imperfect CSI on transmission capacity is shown in Fig. 7, where transmission capacity is plotted for different numbers of antennas per node L . The size of the antenna array is $L = 4$ and the outage constraint is $\epsilon = 10^{-2}$. The length of pilot sequence is $M = \{3, 5, 11\}$. Several observations can be made from Fig. 7. First, the loss on transmission capacity due to CSI reduces as M increases. Such loss is relatively small even for a moderate value of M . For instance, the reduction on transmission capacity is 25% for $M = 11$ and $L = 8$. Second, even for minimum CSI estimation overhead (i.e. $M = 3$), a capacity gain of more than an order of magnitude can be achieved using interference cancellation. This supports the practical applications of interference cancellation. Finally, most capacity gains are contributed by the cancellation of the strongest interferer to each receiving node. The cancellation of more interferers has a much less significant effect on the network capacity since it becomes limited by residual interference.

VII. CONCLUSION

In this paper, a spatial interference cancellation algorithm is applied in a MANET setting and the resulting gains in the network's transmission capacity are characterized under given constraints on the SIR outage probability. Bounds on this outage probability are given for a network with Poisson distributed transmitters. For asymptotically small outage probability, the scaling laws of transmission capacity are derived, which follow the power law for both perfect and imperfect CSI. These scaling laws also accurately predict transmission capacity for the non-asymptotic outage regime. The required lengths of CSI training sequence are derived for constraining the increase of outage probability due to CSI accuracy, and for achieving close-to-optimal capacity scaling laws, respectively. Through simulation, interference

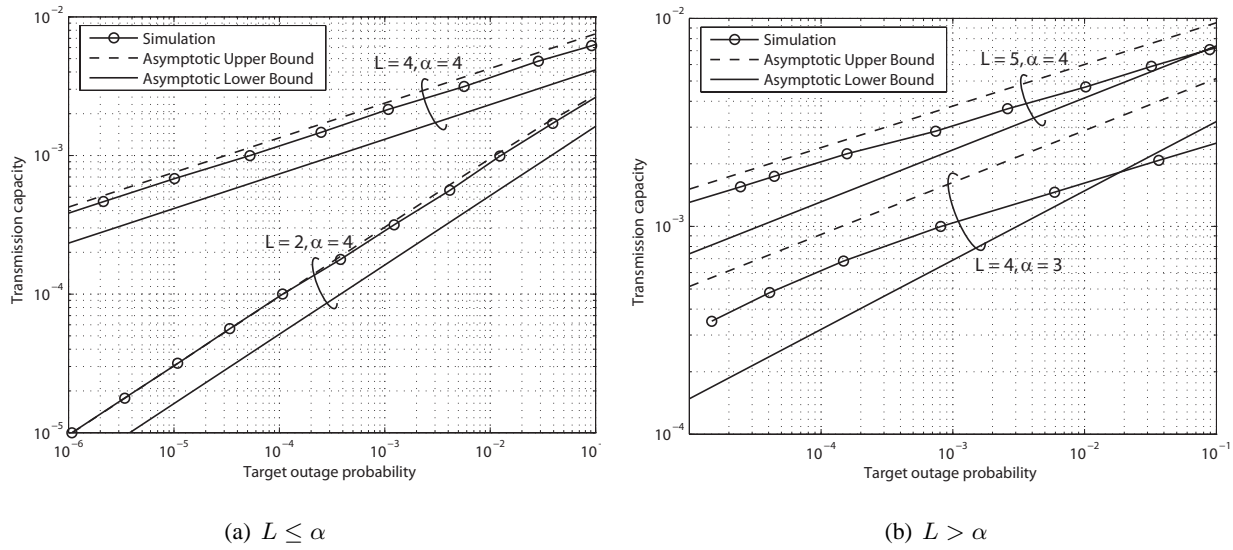


Fig. 5. Comparison between asymptotic bounds on transmission capacity and the exact values obtained by simulation for perfect CSI and the cases of (a) $L < \alpha$ and (b) $L \geq \alpha$.

cancellation are observed to provide significant network capacity gains even for just a few (2–3) antennas per node. As also observed, a moderate amount of CSI training overhead can effectively alleviate the impact of CSI inaccuracy on network transmission capacity. Thus, spatial interference cancellation may be suitable for applications in practical network.

This work opens several issues for future work. First, the bounds on the SIR outage probability derived in this paper provide no simple closed-form expressions. Furthermore, characterizing the asymptotic behavior of the outage probability also seems difficult. Thus, new and more powerful analytical tools should be found if possible. Second, integration of interference cancellation and stream control [42] provides additional gains on network transmission capacity. Last, it is useful to investigate the performance of interference cancellation for ad hoc networks in more realistic settings such as heterogeneous traffic patterns and high mobility.

ACKNOWLEDGEMENT

The authors thank Dr. Gustavo de Veciana and Dr. Nihar Jindal for helpful discussions.

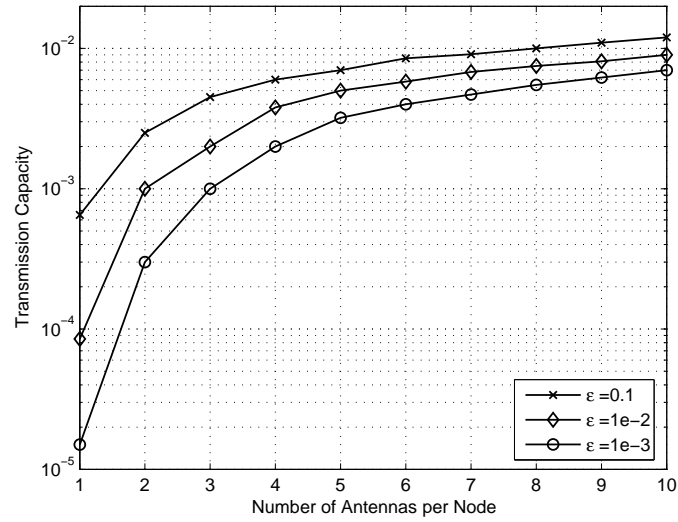


Fig. 6. Transmission capacity by simulation for different node densities and perfect CSI. The size of the antenna array is $L = 4$ and the outage constraint is $\epsilon = \{10^{-1}, 10^{-2}, 10^{-3}\}$.

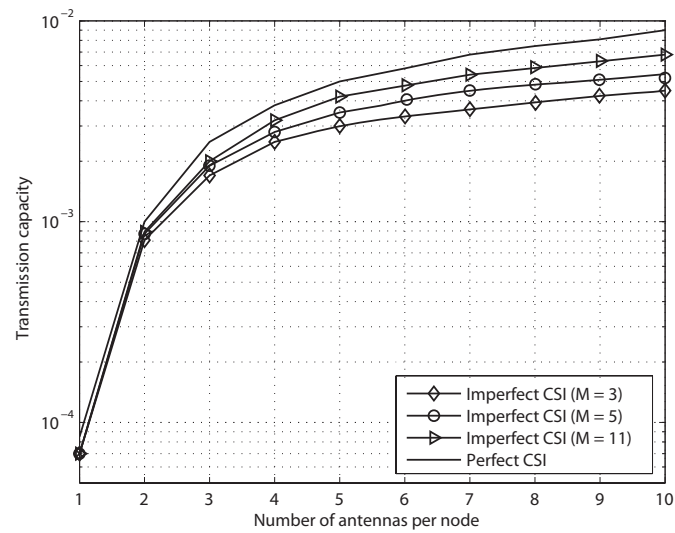


Fig. 7. Transmission capacity by simulation for different node densities and imperfect CSI. The size of the antenna array is $L = 4$ and the outage constraint is $\epsilon = 10^{-2}$.

APPENDIX

A. Proof of Lemma 2

Define a marked Poisson point process as $\mathcal{M}(g) = \{(T_n, I_n) \mid T_n \in \Phi / \{T_0\}, I_n \geq g\}$. Given that $I_n = r_n^{-\alpha} \rho_n$, the node density of $\mathcal{M}(g)$ follows from the Marking Theorem as

$$\begin{aligned} \mu(\mathcal{M}(g)) &= \lambda \int_0^\infty \int_0^{(t/g)^{1/\alpha}} 2\pi r f_\rho(t) dr dt \\ &= \pi \lambda g^{-\delta} \int_0^\infty t^\delta e^{-t} dt \\ &= \nu \lambda g^{-\delta}. \end{aligned} \quad (32)$$

where δ and ν are defined in the statement of the lemma. The cumulative density function of G is the probability that the number of nodes in the subset $\mathcal{M}(g)$ is no more than $(L-1)$. Thus,

$$\Pr(G \leq g) = \sum_{k=0}^{L-1} \frac{(\nu \lambda g^{-\delta})^k}{k!} \exp(-\nu \lambda g^{-\delta}). \quad (33)$$

The probability density function of G is obtained by differentiating the above function

$$\begin{aligned} f_G(g) &= \delta \sum_{k=0}^{L-1} \frac{(\nu \lambda)^{k+1}}{k!} g^{-\delta(k+1)-1} e^{-\nu \lambda g^{-\delta}} - \delta \sum_{k=1}^{L-1} \frac{(\nu \lambda)^k}{(k-1)!} g^{-\delta k-1} e^{-\nu \lambda g^{-\delta}} \\ &= \delta e^{-\nu \lambda g^{-\delta}} \left\{ \sum_{k=0}^{L-1} \frac{(\nu \lambda)^{k+1}}{k!} g^{-\delta(k+1)-1} - \delta \sum_{k=0}^{L-2} \frac{(\nu \lambda)^{k+1}}{k!} g^{-\delta(k+1)-1} \right\}. \end{aligned}$$

The desired result follows from the last equation.

Using Campbell's theorem [39], the expressions for $\text{Var}(I_\Pi(g))$ and $\mathbf{E}[I_\Pi(g)]$ are obtained as

$$\begin{aligned} \mathbf{E}[I_\Pi \mid g] &= 2\pi \lambda \int_0^\infty \int_{\left(\frac{\rho}{g}\right)^{1/\alpha}}^\infty r^{1-\alpha} \rho e^{-\rho} dr d\rho \\ &= \frac{2\lambda\nu}{\alpha-2} g^{1-\delta}. \end{aligned} \quad (34)$$

$$\begin{aligned} \text{Var}(I_\Pi \mid g) &= 2\pi \lambda \int_0^\infty \int_{\left(\frac{\rho}{g}\right)^{1/\alpha}}^\infty r (r^{-\alpha} \rho)^2 e^{-\rho} d\rho dr \\ &= 2\pi \lambda \int_0^\infty \int_{\left(\frac{\rho}{g}\right)^{1/\alpha}}^\infty r^{1-2\alpha} \rho^2 e^{-\rho} dr d\rho \\ &= \frac{\pi \lambda}{\alpha-1} g^{2-\delta} \int_0^\infty \rho^\delta e^{-\rho} d\rho \\ &= \frac{\nu \lambda}{\alpha-1} g^{2-\delta}. \end{aligned} \quad (35)$$

B. Proof of Theorem 1

Define the product space of (W, G) as $\mathcal{D} = [\beta, \infty) \times [0, \infty)$, and $\psi = \theta^{-1}d^{-\alpha}$. The outage probability can be written as

$$P_{\text{out}} = \iint_{(w,g) \in \mathcal{D}} \Pr(I_{\Pi}(g) + g > w) f_W(w) f_G(g) dw dg. \quad (36)$$

As illustrated in Fig. 8, \mathcal{D} is partitioned as $\mathcal{D} = \cup_{n=0}^4 \mathcal{D}_n$ where \mathcal{D}_1 and \mathcal{D}_2 are defined in the statement of the theorem and

$$\mathcal{D}_0 = \{(w, g) \mid 0 \leq g < w\psi, w \geq \beta\} \quad (37)$$

$$\mathcal{D}_3 = \{(w, g) \mid g_0 \leq g < \beta\psi, \beta \leq w \leq g + \mathbf{E}[I_{\Pi}(g)]\} \quad (38)$$

$$\mathcal{D}_4 = \{(w, g) \mid g \geq \beta\psi, g \leq w \leq g + \mathbf{E}[I_{\Pi}(g)]\}. \quad (39)$$

In \mathcal{D}_0 , the primary interference G is sufficiently large for causing an outage. Considering \mathcal{D}_0 alone gives an lower bound on the outage probability denoted as P_{out}^l and given as

$$P_{\text{out}}^l = \iint_{(w,g) \in \mathcal{D}_0} \Pr(I_{\Pi}(g) + g > w) f_W(w) f_G(g) dw dg = \iint_{(w,g) \in \mathcal{D}_0} f_W(w) f_G(g) dw dg. \quad (40)$$

The subset $\mathcal{D}_1 \cup \mathcal{D}_2$ satisfies the criterion for applying Chebyshev's inequality in (20). In $\mathcal{D}_3 \cup \mathcal{D}_4$ where Chebyshev's inequality does not hold, the outage probability is upper bounded as $\Pr(I_{\Pi}(g) + g > w) \leq 1$. Based on the above discussion and (20), an upper bound on the outage probability, denoted as P_{out}^u , is written as

$$P_{\text{out}}^u = P_{\text{out}}^l + \underbrace{\iint_{(w,g) \in \mathcal{D}_1 \cup \mathcal{D}_2} \min\left(\frac{\text{Var}(I_{\Pi}(g))}{(w\psi - g - \mathbf{E}[I_{\Pi}(g)])^2}, 1\right) f_W(w) f_G(g) dw dg}_{\Omega} + \iint_{(w,g) \in \mathcal{D}_3 \cup \mathcal{D}_4} f_W(w) f_G(g) dw dg. \quad (41)$$

The bounds in (40) and (41) are further developed in the following sub-sections.

1) *Lower Bound on Outage Probability:* By substituting (4) and (14) into (40)

$$\begin{aligned} P_{\text{out}}^l &= \frac{\delta \nu^L \lambda^L}{\Gamma(L) P_t} \int_{\psi\beta}^{\infty} \int_{\beta}^{g/\psi} e^{-w} g^{-\delta L-1} e^{-\nu \lambda g^{-\delta}} dw dg \\ &= \frac{\delta \nu^L \lambda^L}{\Gamma(L)} \left[\int_{\psi\beta}^{\infty} g^{-\delta L-1} e^{-\nu \lambda g^{-\delta}} dg - \frac{1}{P_t} \int_{\psi\beta}^{\infty} g^{-\delta L-1} e^{-\nu \lambda g^{-\delta} - \psi^{-1} g} dg \right] \\ &= \frac{1}{\Gamma(L)} \int_0^{\nu \lambda (\beta \psi)^{-\delta}} g^{L-1} e^{-g} dg - \frac{\delta \nu^L \lambda^L}{\Gamma(L) P_t} \int_{\psi\beta}^{\infty} g^{-\delta L-1} e^{-\nu \lambda g^{-\delta} - \psi^{-1} g} dg \\ &= \frac{\gamma(L, \nu \lambda (\beta \psi)^{-\delta})}{\Gamma(L)} - \frac{\delta (\nu \psi^{-\delta})^L \lambda^L}{\Gamma(L) P_t} \int_{\beta}^{\infty} g^{-\delta L-1} e^{-\nu \psi^{-\delta} \lambda g^{-\delta} - g} dg. \end{aligned} \quad (42)$$

The last equation gives the desired lower bound on the outage probability.

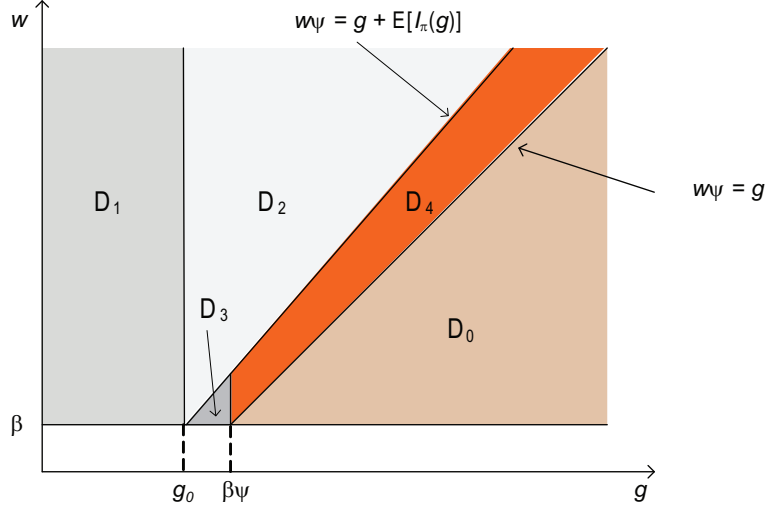


Fig. 8. Partitions in the product space \mathcal{D} (shaded) of (W, G) , which are used to obtain bounds on the outage probability.

2) *Upper Bound on Outage Probability:* From (41)

$$\begin{aligned}
 P_{\text{out}}^u &= P_{\text{out}}^l + \Omega + \int_{\mathcal{D}_3 \cup \mathcal{D}_4} f_W(w) f_G(g) dw dg \\
 &= \Omega + \int_{\mathcal{D}_0 \cup \mathcal{D}_3 \cup \mathcal{D}_4} f_W(w) f_G(g) dw dg \\
 &= \Omega + \int_{g_0}^{\infty} \int_{\beta}^{(g + \frac{2\nu}{\alpha-2} \lambda g^{1-\delta})/\psi} f_W(w) f_G(g) dw dg \\
 &= \underbrace{\Omega + \frac{\delta \nu^L \lambda^L}{\Gamma(L)} \int_{g_0}^{\infty} g^{-\delta L-1} e^{-\nu \lambda g^{-\delta}} dg - \frac{\delta \nu^L \lambda^L}{\Gamma(L) P_t} \int_{g_0}^{\infty} g^{-\delta L-1} e^{-\psi^{-1} g - \frac{2\nu}{\alpha-2} \psi^{-1} \lambda g^{1-\delta} - \nu \lambda g^{-\delta}} dg}_{\tilde{\Omega}}. \quad (43)
 \end{aligned}$$

The desired upper bound follows from the last equation.

C. Proof of Lemma 3

1) *Asymptotic Lower Bound on Outage Probability:* For $\lambda \rightarrow 0$, with c_0 defined following (14), the lower bound on the outage probability in (42) can be rewritten as

$$\begin{aligned}
 P_{\text{out}}^l &= \frac{\delta (\nu \lambda)^L}{P_t \Gamma(L)} \int_{\beta}^{\infty} \int_{w\psi}^{\infty} g^{-\delta L-1} \exp(-\nu \lambda g^{-\delta}) e^{-w} dg dw \\
 &= \frac{\delta (\nu \lambda)^L}{P_t \Gamma(L)} \int_{\beta}^{\infty} \int_{w\psi}^{\infty} g^{-\delta L-1} [1 + O(\lambda)] e^{-w} dg dw \\
 &= \frac{(\nu \psi^{-\delta})^L}{P_t \Gamma(L+1)} \int_{\beta}^{\infty} w^{-\delta L} e^{-w} dw \lambda^L + O(\lambda^{L+1}), \quad \lambda \rightarrow 0 \\
 &= \kappa_1 \lambda^L + O(\lambda^{L+1}), \quad \lambda \rightarrow 0
 \end{aligned} \quad (44)$$

where κ_1 is given in the statement of the lemma.

2) *Asymptotic Upper Bound on Outage Probability*: Define a set and its complementary set, represented by \mathcal{D}_5 and \mathcal{D}_5^c , as follows

$$\mathcal{D}_5 = \left\{ (w, g) \mid w \geq \beta, g + \frac{\delta\nu\lambda}{1-\delta}g^{1-\delta} \leq \frac{w\psi}{2} \right\}, \quad \mathcal{D}_5^c = \left\{ (w, g) \mid w \geq \beta, g + \frac{\delta\nu\lambda}{1-\delta}g^{1-\delta} > \frac{w\psi}{2} \right\}.$$

Moreover, let $\hat{g}(w)$ and $\tilde{g}(w)$ denote the functions that satisfy $\hat{g} + \frac{\delta\nu}{1-\delta}\lambda\hat{g}^{1-\delta} = \frac{w\psi}{2}$ and $\tilde{g} + \frac{\delta\nu}{1-\delta}\lambda\tilde{g}^{1-\delta} = w\psi$, respectively. Note that $\mathcal{D}_5 \in \mathcal{D}_1 \cup \mathcal{D}_2$, where \mathcal{D}_1 and \mathcal{D}_2 are defined in Theorem 1. By using the above definitions, the term Ω defined in (41) can be upper bounded as

$$\begin{aligned} \Omega &\leq \iint_{(w,g) \in (\mathcal{D}_1 \cup \mathcal{D}_2) \cap \mathcal{D}_5} \min \left(\frac{\text{Var}(I_\pi(g))}{(w\psi - g - \mathbf{E}[I_\pi(g)])^2}, 1 \right) f_W(w) f_G(g) dw dg + \\ &\quad \iint_{(w,g) \in (\mathcal{D}_1 \cup \mathcal{D}_2) \cap \mathcal{D}_5^c} f_W(w) f_G(g) dw dg \\ &= \int_{\beta}^{\infty} \int_0^{\hat{g}(w)} \min \left(\frac{\text{Var}(I_\pi(g))}{(w\psi - g - \mathbf{E}[I_\pi(g)])^2}, 1 \right) f_W(w) f_G(g) dw dg + \\ &\quad \int_{\beta}^{\infty} \int_{\hat{g}(w)}^{\tilde{g}(w)} f_W(w) f_G(g) dw dg \\ &\stackrel{(a)}{\leq} \underbrace{\int_{\beta}^{\infty} \int_0^{\hat{g}(w)} \frac{4\delta\nu\lambda g^{2-\delta}}{(2-\delta)(w\psi)^2} f_G(g) f_W(w) dg dw}_{\Lambda_2(\lambda)} + \underbrace{\int_{\beta}^{\infty} \int_{\hat{g}(w)}^{\tilde{g}(w)} f_W(w) f_G(g) dw dg}_{\Lambda_1(\lambda)}, \quad \lambda \rightarrow 0 \end{aligned} \quad (45)$$

Obtaining the inequality (a) uses Lemma 2 and the definition of \hat{g} . By observing that $\hat{g} \leq w\psi/2$ from its definition and substituting (14), $\Lambda_2(\lambda)$ defined in (45) is upper bounded as

$$\begin{aligned} \Lambda_2(\lambda) &\leq \frac{4\delta\nu\psi^{-2}\lambda}{2-\delta} \int_{\beta}^{\infty} w^{-2} \int_0^{\frac{w\psi}{2}} \frac{\delta\nu^L\lambda^L}{\Gamma(L)} g^{-\delta(L+1)+1} \exp(-\nu\lambda g^{-\delta}) dg f_W(w) dw \\ &= \frac{4\delta\psi^{-2}\nu^\alpha\lambda^\alpha}{(2-\delta)\Gamma(L)} \int_{\beta}^{\infty} w^{-2} \underbrace{\int_{\nu\lambda(\frac{w\psi}{2})^{-\delta}}^{\infty} g^{L-\alpha} \exp(-g) dg}_{\Lambda_3(\lambda)} f_W(w) dw. \end{aligned} \quad (46)$$

Note that for $\lambda \rightarrow 0$, $\Lambda_3(\lambda)$ in (46) is bounded for $L \geq \alpha$ and unbounded for $L < \alpha$. It follows from (46) that

$$\Lambda_3(\lambda) \leq \begin{cases} \Gamma(L - \alpha + 1), & L > \alpha \\ (\nu\lambda)^{L-\alpha} \left(\frac{w\psi}{2} \right)^{-\delta L+2} [1 + O(\lambda)], & L \leq \alpha. \end{cases} \quad (47)$$

By substituting (47) into (46)

$$\Lambda_2(\lambda) \leq \begin{cases} \frac{4\delta\psi^{-2}\nu^\alpha\mathbf{E}[W^{-2}]\Gamma(L - \alpha + 1)}{(2-\delta)\Gamma(L)}\lambda^\alpha, & L > \alpha \\ \frac{\delta 2^{\delta L}\psi^{-\delta L}\nu^L\mathbf{E}[W^{-\delta L}]}{(2-\delta)\Gamma(L)}\lambda^L + O(\lambda^{L+1}), & L \leq \alpha. \end{cases} \quad (48)$$

Next, an asymptotic upper bound on $\Lambda_1(\lambda)$ defined in (45) for $\lambda \rightarrow 0$ is obtained as follows. Since $\tilde{g}(w) \leq w\psi$ and $\hat{g}(w) = \frac{w\psi}{2} + O(\lambda)$ from their definitions, by substituting (14), $\Lambda_1(\lambda)$ is bounded as

$$\begin{aligned}
\Lambda_1(\lambda) &\leq \frac{\delta \nu^L \lambda^L}{\Gamma(L)} \int_{\beta}^{\infty} \int_{\frac{w\psi}{2} + O(\lambda)}^{w\psi} g^{-\delta L - 1} \exp(-\nu \lambda g^{-\delta}) dg f_W(w) dw \\
&= \frac{1}{\Gamma(L)} \int_{\beta}^{\infty} \int_{\nu \lambda (w\psi)^{-\delta}}^{\nu \lambda (\frac{w\psi}{2})^{-\delta} + O(\lambda^2)} g^{L-1} \exp(-g) dg f_W(w) dw \\
&\leq \int_{\beta}^{\infty} \frac{[\nu \lambda (\frac{w\psi}{2})^{-\delta} + O(\lambda^2)]^{(L-1)}}{\Gamma(L)} \left[\exp(-\nu \lambda (w\psi)^{-\delta}) - \exp(-\nu \lambda (\frac{w\psi}{2})^{-\delta} + O(\lambda^2)) \right] f_W(w) dw \\
&= \int_{\beta}^{\infty} \frac{\nu^{L-1} \lambda^{L-1} (\frac{w\psi}{2})^{-\delta(L-1)} + O(\lambda^L)}{\Gamma(L)} \left[\nu \lambda (w\psi)^{-\delta} (2^{\delta} - 1) + O(\lambda^2) \right] f_W(w) dw \\
&= \frac{2^{\delta L} (1 - 2^{-\delta}) \nu^L \lambda^L \psi^{-\delta L} \mathbf{E}[W^{-\delta L}]}{\Gamma(L)} + O(\lambda^{L+1}). \tag{49}
\end{aligned}$$

By combining (45), (48), and (49), an asymptotic upper bound for Ω in (41) is obtained as

$$\Omega \leq \begin{cases} \frac{4\delta \psi^{-2} \nu^{\alpha} \mathbf{E}[W^{-2}] \Gamma(L - \alpha + 1)}{(2 - \delta) \Gamma(L)} \lambda^{\alpha}, & L > \alpha \\ 2^{\delta L} \left(\frac{2}{2 - \delta} - 2^{-\delta} \right) \frac{\nu^L \psi^{-\delta L} \mathbf{E}[W^{-\delta L}]}{\Gamma(L)} \lambda^L + O(\lambda^{L+1}), & L \leq \alpha \end{cases} \tag{50}$$

where $\mathbf{E}[W^{-\delta L}] = \Gamma(1 - \delta L, \beta) / P_t$ and $\mathbf{E}[W^{-2}] = \Gamma(-1, \beta) / P_t$.

Finally, using $g_0 = \beta\psi + O(\lambda)$ and following the similar procedure as in Section C.1, it can be shown that $\tilde{\Omega}(\lambda) = \kappa_1 \lambda^L + O(\lambda^{L+1})$, where $\tilde{\Omega}$ is defined in (43). Combining this result, (45) and (50) leads to the desired asymptotic upper bound on the outage probability.

D. Proof of Theorem 3

Using (10) and by definition, the conditional SIR outage probability is given as

$$\begin{aligned}
\Pr(\widetilde{\text{SIR}} \leq \theta) &= \mathbf{E} \left[\Pr(\widetilde{\text{SIR}} \leq \theta \mid \Phi, \{\rho_n\}, W) \right] \\
&= \mathbf{E} \left[\Pr \left(W d^{-\alpha} \theta^{-1} \leq \sigma_r^2 + \sum_{n=L}^{\infty} r_n^{-\alpha} \rho_n \mid \Phi, \{\rho_n\}, W \right) \right] \\
&= \mathbf{E} \left[\Pr \left(W d^{-\alpha} \theta^{-1} \leq \frac{1}{M} \sum_{n=L}^{\infty} r_n^{-\alpha} \rho_n \sum_{l=1}^{L-1} z_l + \sum_{n=L}^{\infty} r_n^{-\alpha} \rho_n \mid \Phi, \{\rho_n\}, W \right) \right] \tag{51}
\end{aligned}$$

where the i.i.d. random variables $\{z_l\}$ follow the exponential distribution with unit mean. Let ζ denote a chi-squared random variable having $(L - 1)$ complex degrees of freedom. It follows from (51) that

$$\Pr(\widetilde{\text{SIR}} \leq \theta) = \mathbf{E} \left[\Pr \left(W d^{-\alpha} \theta^{-1} \leq \sum_{n=L}^{\infty} r_n^{-\alpha} \rho_n \left(1 + \frac{\zeta}{M} \right) \mid \Phi, \{\rho_n\}, W \right) \right]. \tag{52}$$

The above equation can be expanded as

$$\begin{aligned} \Pr(\widetilde{\text{SIR}} \leq \theta) = & \mathbf{E} \left[\Pr \left(W d^{-\alpha} \theta^{-1} \leq \sum_{n=L}^{\infty} r_n^{-\alpha} \rho_n \left(1 + \frac{\zeta}{M} \right) \middle| \Phi, \{\rho_n\}, W, \zeta > Z \right) \right] \Pr(\zeta > Z) + \\ & \mathbf{E} \left[\Pr \left(W d^{-\alpha} \theta^{-1} \leq \sum_{n=L}^{\infty} r_n^{-\alpha} \rho_n \left(1 + \frac{\zeta}{M} \right) \middle| \Phi, \{\rho_n\}, W, \zeta \leq Z \right) \right] \Pr(\zeta \leq Z) \end{aligned} \quad (53)$$

Using the key result in [49], the incomplete Gamma function with $(L-1)$ complex degrees of freedom can be upper bounded as

$$\frac{1}{\Gamma(L-1)} \int_Z^{\infty} \tau^{L-2} e^{-\tau} d\tau \leq 1 - (1 - e^{-\omega Z})^{L-1} \quad (54)$$

where $\omega = [\Gamma(L)]^{-\frac{1}{L-1}}$. By combining (53) and (54)

$$\begin{aligned} \Pr(\widetilde{\text{SIR}} \leq \theta) & \leq \mathbf{E} \left[\Pr \left(W d^{-\alpha} \theta^{-1} \leq \sum_{n=L}^{\infty} r_n^{-\alpha} \rho_n \left(1 + \frac{\zeta}{M} \right) \middle| \Phi, \{\rho_n\}, W, \zeta \leq Z \right) \right] + \\ & \mathbf{E} \left[\Pr \left(W d^{-\alpha} \theta^{-1} \leq \sum_{n=L}^{\infty} r_n^{-\alpha} \rho_n \left(1 + \frac{\zeta}{M} \right) \middle| \Phi, \{\rho_n\}, W, \zeta > Z \right) \right] \times \\ & \sum_{l=1}^{L-1} \binom{L-1}{l} (-1)^l e^{-\omega l Z} \\ & \leq \mathbf{E} \left[\Pr \left(W d^{-\alpha} \theta^{-1} \leq \sum_{n=L}^{\infty} r_n^{-\alpha} \rho_n \left(1 + \frac{Z}{M} \right) \middle| \Phi, \{\rho_n\}, W \right) \right] + \\ & \sum_{l=1}^{L-1} \binom{L-1}{l} (-1)^l e^{-\omega l Z} \\ & \leq \mathbf{E} \left[\Pr \left(W d^{-\alpha} \theta^{-1} \leq \sum_{n=L}^{\infty} r_n^{-\alpha} \rho_n \left(1 + \frac{Z}{M} \right) \middle| \Phi, \{\rho_n\}, W \right) \right] + \\ & \sum_{l=1}^{L-1} \binom{L-1}{l} (-1)^l e^{-\omega l Z}. \end{aligned} \quad (55)$$

Since W follows the exponential distribution,

$$\Pr(W \leq a(1+b)) = \int_0^{a(1+b)} e^{-\tau} d\tau < (1+b) \int_0^a e^{-\tau} d\tau. \quad (56)$$

From (55) and (56)

$$\begin{aligned} \Pr(\widetilde{\text{SIR}} \leq \theta) & \leq \mathbf{E} \left[\Pr \left(W d^{-\alpha} \theta^{-1} \leq \sum_{n=L}^{\infty} r_n^{-\alpha} \rho_n \middle| \Phi, \{\rho_n\}, W \right) \right] \left(1 + \frac{Z}{M} \right) + \\ & \sum_{l=1}^{L-1} \binom{L-1}{l} (-1)^l e^{-\omega l Z} \end{aligned}$$

$$\begin{aligned}
&= \Pr(\text{SIR} \leq \theta) \left(1 + \frac{Z}{M}\right) + \sum_{\ell=1}^{L-1} \binom{L-1}{\ell} (-1)^\ell e^{-\omega \ell Z} \\
&= \Pr(\text{SIR} \leq \theta) \left(1 + \frac{Z}{M}\right) + \sum_{\ell=1}^{L-1} \binom{L-1}{\ell} (-1)^\ell e^{-\omega \ell Z} \\
&= \Pr(\text{SIR} \leq \theta) \left(1 + \frac{Z}{M}\right) + e^{-\omega Z} \sum_{\ell=1}^{L-1} \binom{L-1}{\ell} (-1)^\ell \\
&= \Pr(\text{SIR} \leq \theta) \left(1 + \frac{Z}{M}\right) + 2^{L-1} e^{-\omega Z}.
\end{aligned} \tag{57}$$

The desired result follows from (57).

E. Proof of Theorem 4

By substituting $Z = -\frac{1}{\omega} \log(2^{1-L} \epsilon^2)$ and $M_\epsilon = \frac{Z}{\hat{\varphi}}$ into (28)

$$\tilde{P}_{\text{out}}(M_\epsilon, \lambda) \leq P_{\text{out}}(\lambda) (1 + \hat{\varphi}) + \epsilon^2. \tag{58}$$

To simplify notation, denote $\tilde{P}_{\text{out}}(M_\epsilon, \lambda)$ as $\tilde{P}_{\text{out}}(\lambda)$. Define $\tilde{\lambda}_\epsilon$, $\tilde{\lambda}_\epsilon^l$ and $\tilde{\lambda}_\epsilon^u$ using the equations $\tilde{P}_{\text{out}}(\tilde{\lambda}_\epsilon) = \epsilon$, $P_{\text{out}}(\tilde{\lambda}_\epsilon^u) = \epsilon$ and $P_{\text{out}}(\tilde{\lambda}_\epsilon^l) (1 + \hat{\varphi}) = \epsilon - \epsilon^2$, respectively. These quantities satisfy the relationship $\tilde{\lambda}^l \leq \tilde{\lambda} \leq \tilde{\lambda}^u$. The first inequality is due to that the functions $\tilde{P}_{\text{out}}(\lambda)$ and $P_{\text{out}}(\lambda)$ monotonically decrease with increasing λ ; the second holds since CSI inaccuracy reduces the maximum transmitter density under the outage constraint. For $L \leq \alpha$, using the above inequalities and Theorem 2

$$\lim_{\epsilon \rightarrow 0} \frac{\tilde{C}(M_\epsilon, \epsilon)}{\kappa_2^{-\frac{1}{L}} \epsilon^{\frac{1}{L}}} \geq \lim_{\epsilon \rightarrow 0} \frac{\left[1 - \frac{\epsilon(1-\epsilon)}{1+\hat{\varphi}}\right] \tilde{\lambda}_\epsilon^l}{\kappa_2^{-\frac{1}{L}} [\epsilon(1-\epsilon)]^{\frac{1}{L}}} \geq (1 + \hat{\varphi})^{-1/L} \tag{59}$$

$$\lim_{\epsilon \rightarrow 0} \frac{\tilde{C}(M_\epsilon, \epsilon)}{\kappa_1^{-\frac{1}{L}} \epsilon^{\frac{1}{L}}} \leq \lim_{\epsilon \rightarrow 0} \frac{(1-\epsilon) \tilde{\lambda}_\epsilon^u}{\kappa_1^{-\frac{1}{L}} \epsilon^{\frac{1}{L}}} \leq 1. \tag{60}$$

By substituting $\varphi = (1 + \hat{\varphi})^{-\frac{1}{L}}$ into (59), (60) and $M_\epsilon = -\frac{1}{\hat{\varphi}\omega} \log(2^{1-L} \epsilon^2)$ and taking into account that $M_\epsilon \geq L - 1$ is an integer, the desired result for $L \geq \alpha$ follows. The result for $L > \alpha$ is derived following the same procedure.

REFERENCES

- [1] S. Weber, J. G. Andrews, and N. Jindal, "The effect of fading, channel inversion, and threshold scheduling on ad hoc networks," *IEEE Trans. on Info. Theory*, vol. 53, pp. 4127–4149, Nov. 2007.
- [2] S. P. Weber, X. Yang, J. G. Andrews, and G. de Veciana, "Transmission capacity of wireless ad hoc networks with outage constraints," *IEEE Trans. on Info. Theory*, vol. 51, pp. 4091–02, Dec. 2005.
- [3] A. Hasan and J. G. Andrews, "The guard zone in wireless ad hoc networks," *IEEE Trans. on Wireless Communications*, vol. 6, pp. 897–906, Mar. 2007.
- [4] R. K. Ganti and M. Haenggi, "Regularity, interference, and capacity of large ad hoc networks," in *Proc., IEEE Asilomar*, Oct. 2006.

- [5] J. Venkataraman, M. Haenggi, and O. Collins, "Shot noise models for the dual problems of cooperative coverage and outage in random networks," in *Proc., Allerton Conf. on Comm., Control, and Computing*, Sept. 2006.
- [6] N. Jindal, J. Andrews, and S. Weber, "Bandwidth partitioning in decentralized wireless networks," *submitted to IEEE Trans. on Wireless Communications*, Nov. 2007.
- [7] S. Weber, J. G. Andrews, X. Yang, and G. de Veciana, "Transmission capacity of wireless ad hoc networks with successive interference cancellation," *IEEE Trans. on Info. Theory*, vol. 53, pp. 2799–2814, Aug. 2007.
- [8] P. Gupta and P. R. Kumar, "The capacity of wireless networks," *IEEE Trans. on Info. Theory*, vol. 46, pp. 388–404, Mar. 2000.
- [9] M. Grossglauser and D. N. C. Tse, "Mobility increases the capacity of ad hoc wireless networks," *IEEE Trans. on Networking*, vol. 10, pp. 477–486, Aug. 2002.
- [10] M. Franceschetti, O. Dousse, D. N. C. Tse, and P. Thiran, "Closing the gap in the capacity of wireless networks via percolation theory," *IEEE Trans. on Info. Theory*, vol. 53, pp. 1009–18, Mar. 2007.
- [11] A. Jovicic, P. Viswanath, and S. R. Kulkarni, "Upper bounds to transport capacity of wireless networks," *IEEE Trans. on Info. Theory*, vol. 50, pp. 2555–65, Nov. 2004.
- [12] F. Xue, L.-L. Xie, and P. R. Kumar, "The transport capacity of wireless networks over fading channels," *IEEE Trans. on Info. Theory*, vol. 51, pp. 834–847, Mar. 2005.
- [13] A. Ozgur, O. Leveque, and D. N. C. Tse, "Hierarchical cooperation achieves optimal capacity scaling in ad hoc networks," *IEEE Trans. on Info. Theory*, vol. 53, pp. 3549–3572, Oct. 2007.
- [14] V. R. Cadambe and S. A. Jafar, "Interference alignment and the degrees of freedom for the k user interference channel," *Preprint: <http://arXiv.org:0707.0323>*, July 2007.
- [15] A. Goldsmith, *Wireless Communications*. Cambridge University Press, 2005.
- [16] S. Kumar, V. S. Raghavan, and J. Deng, "Medium access control protocols for ad hoc wireless networks: A survey," *Ad Hoc Networks*, vol. 4, pp. 326–358, May 2006.
- [17] M. Zorzi, J. Zeidler, A. Anderson, B. Rao, J. Proakis, A. L. Swindlehurst, M. Jensen, and S. Krishnamurthy, "Cross-layer issues in MAC protocol design for MIMO ad hoc networks," *IEEE Wireless Communications Magazine*, vol. 13, pp. 62–76, Aug. 2006.
- [18] B. Hamdaoui and K. G. Shin, "Characterization and analysis of multi-hop wireless mimo network throughput," in *Proc., ACM Intl. Symposium on Mobile Ad Hoc Networking and Computing*, pp. 120–129, 2007.
- [19] J. C. Mundarath, P. Ramanathan, and B. D. V. Veen, "A cross layer scheme for adaptive antenna array based wireless ad hoc networks in multipath environments," *Wireless Networks*, vol. 13, no. 5, pp. 597–615, 2007.
- [20] J.-S. Park, A. Nandan, M. Gerla, and H. Lee, "SPACE-MAC: enabling spatial reuse using MIMO channel-aware MAC," in *Proc., IEEE Intl. Conf. on Communications*, vol. 5, pp. 3642–3646, May 2005.
- [21] M. Z. Siam, M. Krunz, A. Muqattash, and S. Cui, "Adaptive multi-antenna power control in wireless networks," in *Proc., Intl. Conf. on Wireless Comm. and Mobile Computing*, pp. 875–880, 2006.
- [22] Z. Huang, Z. Zhang, and B. Ryu, "Power control for directional antenna-based mobile ad hoc networks," in *Proc., Intl. Conf. on Wireless Comm. and Mobile Computing*, pp. 917–922, 2006.
- [23] R. Ramanathan, J. Redi, C. Santivanez, D. Wiggins, and S. Polit, "Ad hoc networking with directional antennas: a complete system solution," *IEEE Journal on Selected Areas in Communications*, vol. 23, pp. 496–506, Mar. 2005.
- [24] A. Deopura and A. Ganz, "Provisioning link layer proportional service differentiation in wireless networks with smart antennas," *Wireless Networks*, vol. 13, no. 3, 2007.
- [25] K. Sundaresan and R. Sivakumar, "A unified mac layer framework for ad-hoc networks with smart antennas," in *Proc., ACM Intl. Symposium on Mobile Ad Hoc Networking and Computing*, pp. 244–255, 2004.
- [26] H. Singh and S. Singh, "Smart-ALOHA for multi-hop wireless networks," *Mobile Networks and Applications*, vol. 10, no. 5, pp. 651–662, 2005.

- [27] R. Ramanathan, "On the performance of ad hoc networks with beamforming antennas," in *Proc., ACM Intl. Symposium on Mobile Ad Hoc Networking and Computing*, pp. 95–105, 2001.
- [28] A. Singh, P. Ramanathan, and B. Van Veen, "Spatial reuse through adaptive interference cancellation in multi-antenna wireless networks," in *Proc., IEEE Globecom*, vol. 5, Nov. 2005.
- [29] T. Joshi, H. Gossain, C. C., and D. P. Agrawal, "Route recovery mechanisms for ad hoc networks equipped with switched single beam antennas," in *Proc., Annual Symposium on Simulation*, 2005.
- [30] Y. Wu, L. Zhang, Y. Wu, and Z. Niu, "Interest dissemination with directional antennas for wireless sensor networks with mobile sinks," in *Proc., Intl. Conf. on Embedded networked sensor systems*, pp. 99–111, 2006.
- [31] C. M. Yago and P. M. Ruiz, "Energy-efficient multicast with directional antennae and localized tree reconfiguration," in *Proc., ACM Intl. Symposium on Model., Analysis & Simulation of Wireless & Mobile Systems*, pp. 151–154, 2006.
- [32] K. Sundaresan, W. Wang, and S. Eidenbenz, "Algorithmic aspects of communication in ad-hoc networks with smart antennas," in *Proc., ACM Intl. Symposium on Mobile Ad Hoc Networking and Computing*, pp. 298–309, 2006.
- [33] R. Vilzmann, C. Bettstetter, D. M., and C. Hartmann, "Hop distances and flooding in wireless multihop networks with randomized beamforming," in *Proc., ACM Intl. Symposium on Model., Analysis & Simulation of Wireless & Mobile Systems*, pp. 20–27, 2005.
- [34] J. Zhang and S. C. Liew, "Capacity improvement of wireless ad hoc networks with directional antennae," *SIGMOBILE Mobile Computing Comm. Review*, vol. 10, no. 4, 2006.
- [35] S. Yi, Y. Pei, S. Kalyanaraman, and B. Azimi-Sadjadi, "How is the capacity of ad hoc networks improved with directional antennas?," *Wireless Networks*, vol. 13, no. 5, pp. 635–648, 2007.
- [36] A. M. Hunter, J. G. Andrews, and S. P. Weber, "Transmission capacity of ad hoc networks with spatial diversity," *to appear IEEE Trans. on Wireless Communications*.
- [37] F. Baccelli, B. Blaszczyszyn, and P. Muhlethaler, "An ALOHA protocol for multihop mobile wireless networks," *IEEE Trans. on Info. Theory*, vol. 52, pp. 421–36, Feb. 2006.
- [38] J. F. C. Kingman, *Poisson processes*. Oxford University Press, 1993.
- [39] D. Stoyan, W. S. Kendall, and J. Mecke, *Stochastic Gemoetry and its Applications*. Wiley, 2nd ed., 1995.
- [40] V. Tarokh, H. Jafarkhani, and A. R. Calderbank, "Space-time block codes from orthogonal designs," *IEEE Trans. on Info. Theory*, vol. 45, pp. 1456–1467, Jul. 1999.
- [41] I. E. Telatar, "Capacity of multi-antenna Gaussian channels," *European Trans. on Telecomm.*, vol. 10, no. 6, pp. 585–595, 1999.
- [42] K. Sundaresan, R. Sivakumar, M. A. Ingram, and T.-Y. Chang, "Medium access control in ad hoc networks with MIMO links: optimization considerations and algorithms," *IEEE Trans. on Mobile Computing*, vol. 3, no. 4, pp. 350–365, 2004.
- [43] T. K. Y. Lo, "Maximum ratio transmission," *IEEE Trans. on Communications*, vol. 47, pp. 1458–1461, Oct. 1999.
- [44] A. J. Goldsmith and P. Varaiya, "Capacity of fading channels with channel side information," *IEEE Trans. on Info. Theory*, vol. 43, pp. 1986–92, Nov. 1997.
- [45] G. Caire, G. Taricco, and E. Biglieri, "Optimum power control over fading channels," *IEEE Trans. on Info. Theory*, vol. 45, pp. 1468–89, July 1999.
- [46] T. L. Marzetta and B. M. Hochwald, "Fast transfer of channel state information in wireless systems," *IEEE Trans. on Signal Processing*, vol. 54, pp. 1268–78, Apr. 2006.
- [47] S. B. Lowen and M. C. Teich, "Power-law shot noise," *IEEE Trans. on Info. Theory*, vol. 36, pp. 1302–18, Nov. 1990.
- [48] S. Weber and M. Kam, "Computational complexity of outage probability simulations in mobile ad-hoc networks," in *Proc., Conf. on Information Sciences and Systems*, Mar. 2005.
- [49] H. Alzer, "On some inequalities for the incomplete Gamma function," *Mathematics of Computation*, vol. 66, pp. 771–778, Apr. 2005.